Final Technical Report (FTR)

Agency/Office/Program	DOE/EERE/Solar Energy Technology Office	
Award Number	DE-EE0008994	
Project Title	Creep and Fatigue Characterization of High Strength Alloy Thin Sections in Advanced CO2 Heat Exchangers	
Principal Investigator	Jake Boxleitner, Mechanical Engineer jake.boxleitner@braytonenergy.com (603) 601-0450	
Business Contact	Jim Nash, Engineering Director nash@braytonenergy.com (603) 601-0450	
Submission Date	May 27, 2022	
DUNS Number	-	
Recipient Organization	Brayton Energy and Oak Ridge National Laboratory	
Project Period	**Start:** 04/01/20	**End:** 04/29/22
Project Expenditure	Total $600,949 (DOE: $429,184; C/S: $171,765)	
Submitting Official Signature	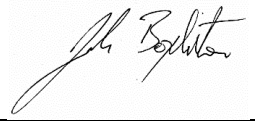	

1. Acknowledgement

This material is based upon work supported by the U.S. Department of Energy's Office of Energy Efficiency and Renewable Energy (EERE) under the SETO Fiscal Year 2019 Funding Program DE-FOA-0002064 Award Number DE-EE0008994.

2. Disclaimer

3. Executive Summary

Project Objectives

Goal: Characterize and model elevated temperature creep and fatigue behavior for thin sheet and foil forms of γ'alloys 740H and 282 in wrought and as-processed form with application in folded and brazed constructions.

Innovation: Gamma-prime strengthened alloys represent a step-change in raw-material strength over solid-solution strengthened alloys.

The folded-fin and brazed plate heat exchanger architecture is remarkably light-weight and leverages cost-effect material stock product forms.

Approach

What:	Folded fin and brazed plate heat exchangers for supercritical CO2 applications
Why:	(1) Haynes 282 and Inconel 740H exhibit increased allowable stress under typical service conditions (2) Architecture employs economic material form factors to create a light and thermally responsive HX
Challenge:	(1) Elevated temperature performance in foil form is previously unquantified (2) Titanium and Aluminum oxides challenge the typically employed vacuum brazing process
How:	Material characterization and manufacturing trials

Key Accomplishments to Date

- 14 uniaxial creep tests completed with Haynes 282 foils
- 11 pressurized creep and fatigue tests completed successfully with Haynes 282 heat exchanger prototypes. Quantity 4 on-going tests.

End of Project Goals

- Haynes 282 foils have been demonstrated to yield rupture times two to three orders of magnitude higher than Haynes 230 under similar conditions
- Physics CDM-based creep modeling can capture both thick and thin form performance, model and data times to failure agree within 15%.
- Manufacturing structural heat exchanger geometries has been supported by pressurized creep testing. Models and data times to failure agree within 27%
- Haynes 282 PHX thermal-hydraulic performance offers ~18% cost savings over Haynes 230 at the same conditions and/or the ability to operate at higher temp

Path Forward

- The technology is technically sound, but the market needs affirmation in this non-traditional architecture for high-temperature, high-pressure applications.
- The path forward includes continued development in prototype and low-quantity production applications while the technology tries to find a home.
- The market is interested in the light-weight architecture and potential cost savings, investment in a code-qualification or larger scale demonstration is likely needed

4. Table of Contents

1. Background:

Technical background is provided in 7. Project Results and Discussion subsection a. Task 1: Project setup subsection i. Subtask 1.1.

2. Project Objectives

a. Project Motivation

What	Folded fin and brazed plate heat exchangers for supercritical CO2 applications
Why	1. Haynes 282 and Inconel 740H exhibit increased allowable stress under typical service conditions 2. Architecture employs economic material form factors to create a light and thermally responsive HX
The Challenge	1. Elevated temperature performance in foil form is previously unquantified 2. Titanium and Aluminum oxides challenge the typically employed vacuum brazing process
How	Material characterization and manufacturing trials

b. Statement of Project Objectives (SOPO) Summary

Characterize and model elevated temperature creep and fatigue behavior for thin sheet and foil forms of γ'alloys 740H and 282 in wrought and as-processed form with application in folded and brazed constructions.

The data base, successfully executed, will provide designers of structures specifying these alloys in thin sheet and foil the means to assess creep and fatigue life with a quantified statistical confidence. The data base will extend into a subclass of structures in which fin folding and Ni-brazing are used in processing.

Structural, thermo-hydraulic, and economic heat exchanger models are to benchmark γ'alloy construction leveraging results from the test campaign.

c. Technical Work Plan

This project is partitioned into three tasks. Task 1 is labeled as the project setup and management task linking Task 2 and Task 3. Task 2 is classified as a fundamental development primarily being executed at ORNL on foil fundamentals. Task 3 is a practical development primarily being executed at Brayton Energy on as-manufacture plate and in heat exchangers.

Project structure is as follows.

Task 1: Project setup and management
- Subtask 1.1: Finalization of scope and test matrices
- Subtask 1.2: Alloy procurement
- Subtask 1.3: Project management

Task 2: Uniaxial creep testing, metallography, and modeling
- Subtask 2.1: As-received material benchmark
- Subtask 2.2: Uniaxial creep testing
- Subtask 2.3: Failure analysis
- Subtask 2.4: Oxidation, corrosion, and physics-based modeling

Task 3: As-processed testing, metallography, and modeling
- Subtask 3.1: Test article definitions
- Subtask 3.2: Manufacturing process validation
- Subtask 3.3: Test article fabrication
- Subtask 3.4: Pressurized creep testing
- Subtask 3.5: Pressurized creep testing failure analysis
- Subtask 3.6: Pressurized creep-fatigue testing
- Subtask 3.7: Pressurized creep-fatigue testing failure analysis
- Subtask 3.8: Heat exchanger benchmark and modeling

The next section will outline details in each subtask in more detail. Additionally, milestones, go/no-go decision points, and end-of-project goals will be discussed in the next section.

5. Project Results and Discussion

The content in this results and discussion narrative section is presented serially by task number.

a. Task 1: Project Setup

i. Subtask 1.1: Background and definition of scope

Fundamental Development

The *fundamental* development isolates material form thickness from manufacture. In this development path, uniaxial creep testing of thin sheet and foil places emphasis on the raw elevated temperature capability of the materials and serves as a baseline for the practical development.

For the fundamental development technical parameters of interest most notably include grain size and form thickness. Quantified elevated temperature performance in the relevant thin sheet and foil form factor has been previously documented for alloy 230, 282, 625, 700, Hastelloy-X, and Waspoloy [1, 4, 8, 11]. Leveraging said documentation and existing thick-form behavior for Inconel 740, the performance decrement expected with decreasing form thickness is established in this section and used to guide test campaign specifications. Alloy 625 possesses has the most expansive characterization while the remaining alloys are referenced in isolation.

Stress-rupture and Larson-Miller Parameter (LMP) data points for alloy 625 and 230 .003-.005” foil is presented in Figure 1a alongside thick form nominal trend lines [1, 16, 18]. Figure annotation “Line D,” highlights the debit observed as a result of the thin form factor and corresponding grain size effect. Average foil grain sizes for alloy 625 were approximately 10µm versus 100+µm for the thick form trend [1, 19].

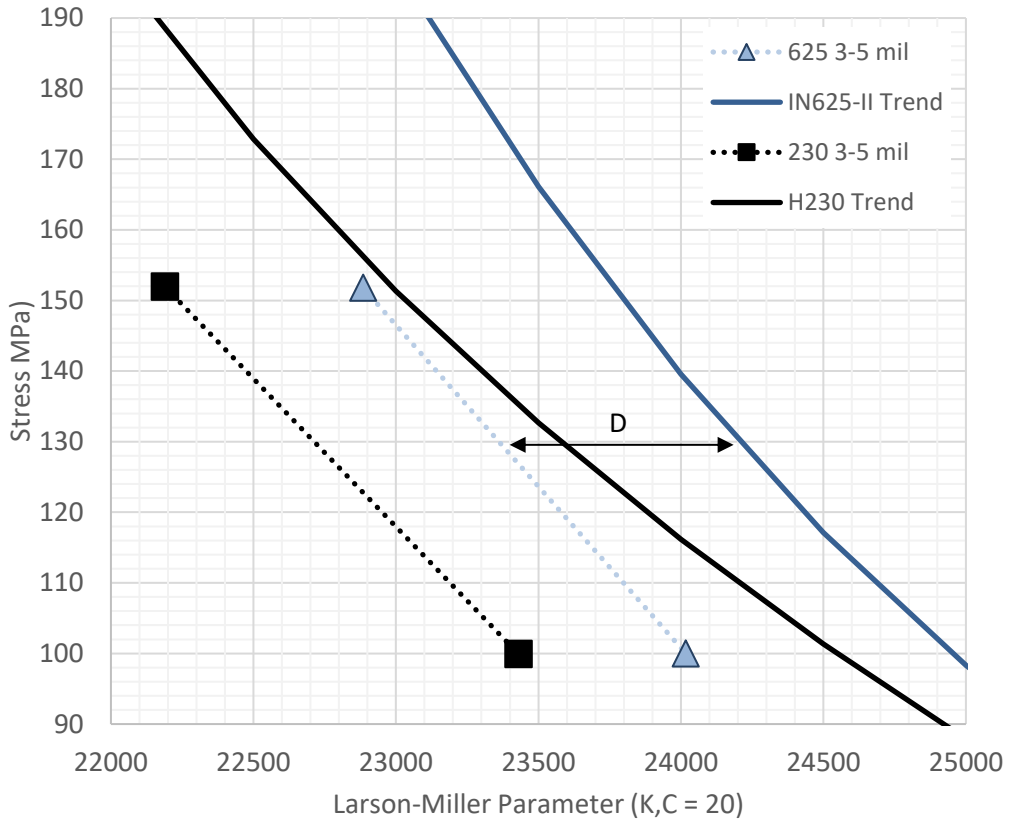

Figure 1: (a) Stress-rupture versus Larson-Miller Parameter for 3-5 mil alloy 625 and 230 foils relative to thick form trends (b) Normalized Larson-Miller Parameter sigmoid debit as a function of form thickness assuming near-constant grain size.

Stress-rupture and Larson-Miller data points for alloy 625 .025" (1 mm) sheet are presented in Figure 2[8]. The samples were given three different heat treatments, each with a corresponding grain size yield. The implications on heat treatment and the grain size effect are then compared to thick form trend lines of alloy 625 Grade I and Grade II. The most notable take away from this test data is the relationship between grain size and the LMP. In the mill-annealed condition (Case A), average grain size is 30µm and stress-rupture trends similar with the Grade I condition. In the 1100°C solution anneal (Case B), average grain size is 100µm and stress rupture trends between the Grade I and Grade II condition. In the 1150°C solution anneal condition (Case C), average grain size is 300µm and stress-rupture trends similar with a decremented Grade II condition. The grain count through test specimen thickness for case A, B, and C is 21.1, 6.4, and 2.1 respectively. It is clear that scatter exists in the data set, specifically with regard to Case B, but unclear as to why. Practically speaking, between six and ten grains are desired through form thickness to ensure reliability of the desired failure mechanisms. Case C, reinforces the grain size effect but uncertainty exists with slightly more than two grains through the thickness. In service, such few grains through the thickness exposes the material to increased fatigue failure risk. For this reason, the six plus grains through form thickness will be targeted in this development.

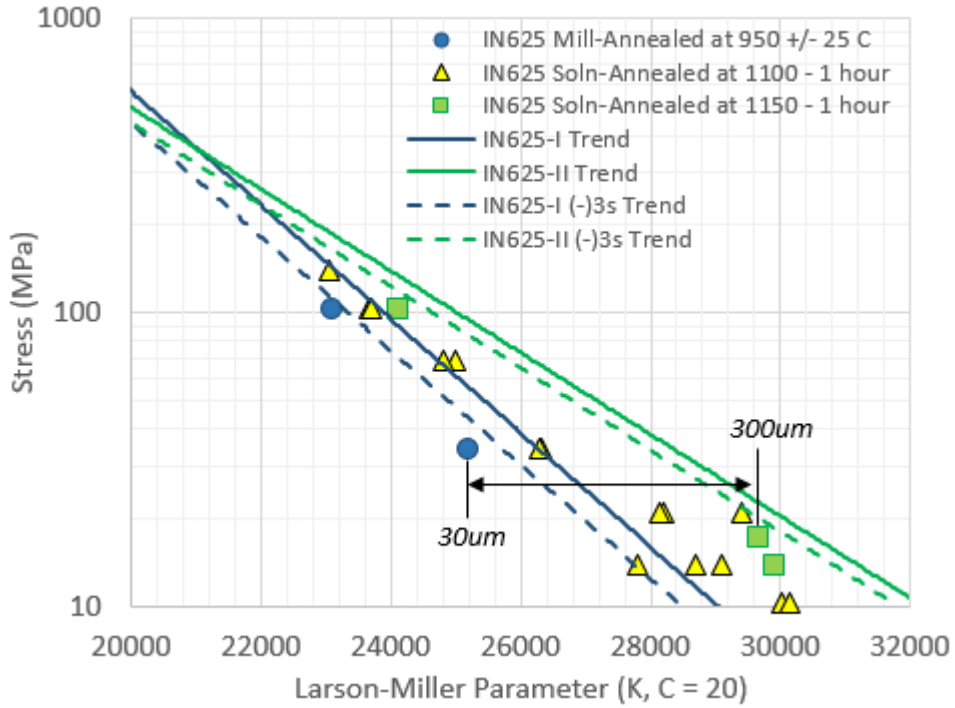

Figure 2: Alloy 625 thin sheet stress-rupture as a function of heat treatment and corresponding grain size [8]

The implications of heat treatment evident with alloy 625 with be discussed further in the *Practical Development* section as pertains to alloy 282 and 740. In short, depending on the condition of the as-received materials, heat treatment and aging will be used to optimize the microstructure for high temperature service.

Practical Development

The *practical* development employs manufacturing practice. In this development path, cold work, heat treat, and braze cycles aim to match parent material elevated temperature performance in the form of pressure creep and creep-fatigue of as-manufactured unit cell geometry.

Forming strain is relevant in two aspects of these thin sheet structures: in the initial rolling of the material and in the folding of fin. In both cases, detrimental effect on elevated temperature performance is observed [3, 6, 20]. The derived relationship between cold strain and creep rupture for alloy 740 is presented in Figure 3, the data has been normalized with respect to unstrained test specimen. On the secondary axis is folded fin density as a function of cold strain for two different fin thickness specifications. Supercritical CO2 applications typically require fin densities ranging between 40 and 55 fins per inch, depending on the service operating conditions and material specification.

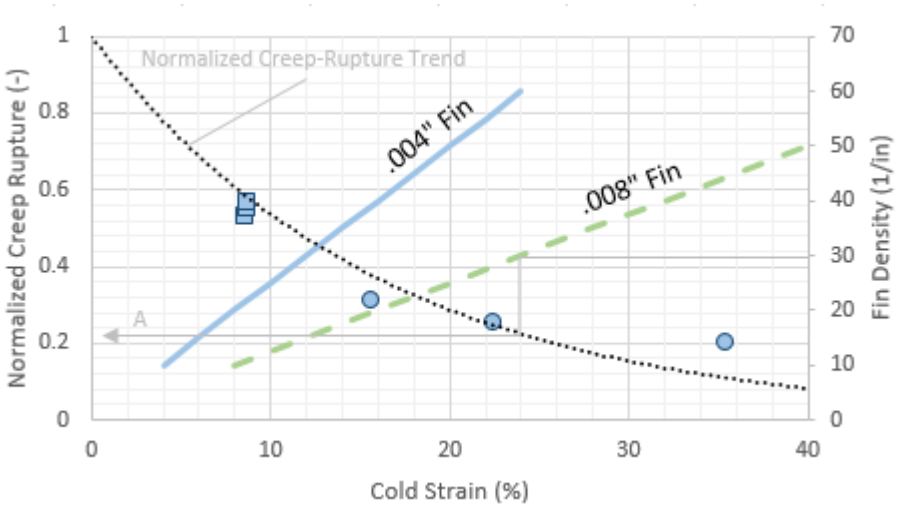

Figure 3: Cold strain implications on creep-rupture behavior and corresponding cold strain given fin thickness and fin density specification [3, 20].

Line A denotes a .008” fin thickness and 30 fins per inch specification and the resultant 24% cold strain and ~80% reduction in creep-rupture behavior. This highlights the importance in understanding the microstructure state post cold strain and heat treat. In Task 3 Subtask 3.2, metallographic examination of this microstructure will be conducted to investigate and quantify notable observations. Details regarding heat treatment will be discussed in the following section as pertains to the braze cycle.

Brazing alloys with high levels of titanium and aluminum introduces complications with respect to titanium and aluminum oxides inhibiting braze alloy surface wetting and therefore bond strength. Nominal compositions of Haynes 282 and Inconel 740H are shown in Table 1. Titanium and Aluminum content of these alloys along with other common aerospace and gas-turbine Ni-based alloys are shown in Figure 4. Braze and weld lines segregate the alloys by viable means of joining [12]. Braze joint wetting becomes problematic when aluminum and titanium composition exceed 0.4% by weight [21]. Note the relative location of alloys 282 and 740.

Table 1: Haynes 282 and Inconel 740 Nominal Compositions [15, 17]

Nominal Composition Values			
Element		282	740
Nickel	Ni	Bal.	Bal.
Chromium	Cr	20	24.5
Iron	Fe	1.5	
Molybdenum	Mo	8.5	0.1
Niobium	Nb		1.5
Carbon	C	0.06	0.03
Manganese	Mn	0.3	
Silicon	Si	0.15	0.15
Aluminum	Al	1.5	2
Titanium	Ti	2.1	1.35
Cobalt	Co	10	20
Boron	B	0.005	

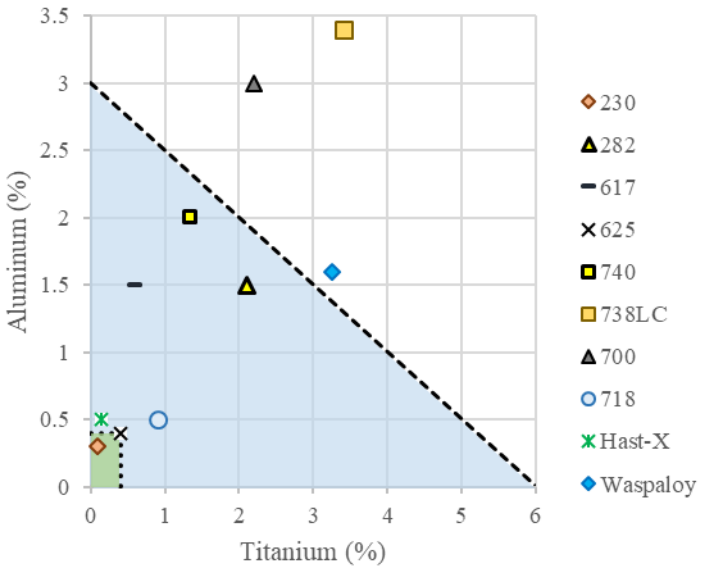

Figure 4: Several nickel alloy titanium and aluminum contents with typical brazing and welding line divisions[12].

The metal-oxide equilibrium curves, Figure 5, are used to visualize this challenge as well as provide guidance to a solution [22]. Typical braze furnace vacuum targets 10^{-4} torr and Ni-brazing temperatures range from 950-1200°C, denoted region “B” in the figure. Relative to this region, the location of titanium and aluminum suggest increased temperature and vacuum is needed to be reduced but this situation is unrealistic and unattainable. However, the relative location of Zirconium may offer permit the use of brazing getters as a potential solution to this oxide problem – to be discussed in the following section.

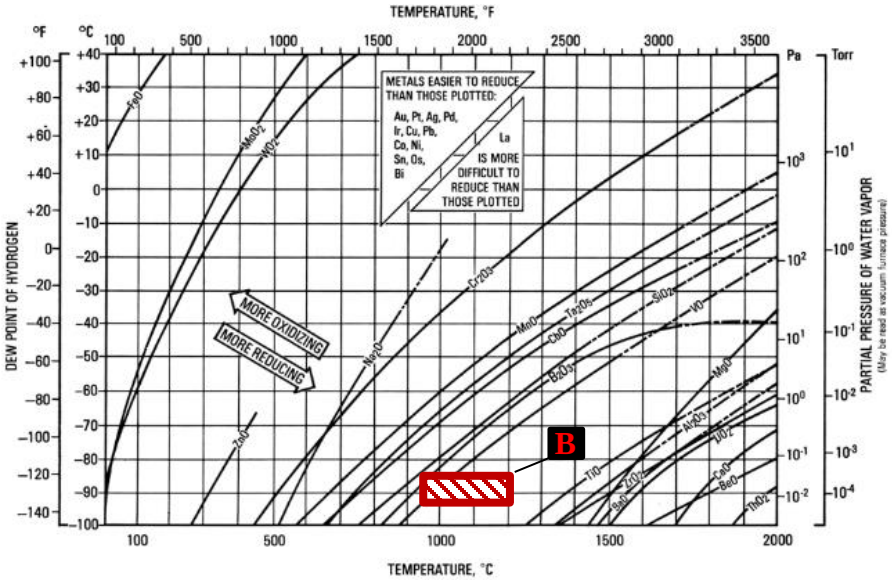

Figure 5: Metal-Metal Oxide Equilibria in Pure Hydrogen Atmospheres [22]

Because titanium and aluminum oxides are inherent in this processing, two approaches are considered to overcome the challenges they introduce, in order of technical preference.

1. Ni-Plating is recommended for brazing alloys containing greater than 0.4% aluminum or titanium and common amongst alloys presented in Figure 4. [4, 11, 21]. Two types of Ni-Plating processes are considered:
    a. Electrolytic Ni-plating uses electricity in a chemical bath to deposit a layer of pure nickel onto a substrate. Due to the high liquidus (1455°C) of this plating, consideration is given to plating thickness and braze alloy specification. An appropriate plating thickness must allow for diffusion of the parent material at solution anneal and brazing temperatures. Additionally, braze alloy sheet or paste must also be applied adding to the cost of this solution.

       The preferred brazing approach for this manufacturing development is as follows:
        a. Prepare the desired geometry – fin folding and plate cutting
        b. Preferentially or fully plate the brazed joint interfaces
        c. Heat treatment to prepare the microstructure for braze diffusion
        d. Braze the unit cell geometry with BNi5a .0015”foil

       This process was proven successful in the development of Inconel 700 brazing with applications in air cooled turbine blades, nuclear reactor heat exchangers, and supersonic aircraft and space vehicles [11]. In the referenced development, .030” sheet and .0002-.0004” electrolytic plate was shown to outperform parent material in the as-received condition with processing in accordance to the above outline. Similar braze alloy contents will be used as they have also shown success in other studies [11, 12] as well

as in practice at Brayton Energy. Solution anneal heat treatment will be ideal but grain growth management will be required. Heat treatment temperature will be specified after as-received benchmark at ORNL.

This approach is justified due to the positive instance observed with alloy 700 and the number of instances of failure when brazing without plating. Recommended plating thickness range between .0002 and .0015" at joint interfaces, this number is to be discussed with the plating supplier [21]

b. Electroless Ni-Plating chemically deposits a Nickel-Phosphorous (NiP) (BNi6 similar) braze alloy compound onto the desired surface. The Phosphorous element of the compound acts as a melt depressant and near 900°C, the plated compound enters liquidus phase wicking the to-be-brazed surface, provided appropriate plating thickness specification. A concern with this approach is the brazing temperature set by the NiP plating. A diffusion hold brazing process has proven successful in prior trials for Haynes 230, for this reason similar approach is preferred with Haynes 282 and Inconel 740H. A diffusion hold temperature of 1130°C for Haynes 282 has been shown to eliminate brazed joint eutectics [10]. Additionally, if more than one braze cycles are needed in bonding of components this temperature limits the number of available alloys to employ.

Both nickel plating options add to the overall processing costs associated with manufacture but may be a necessary step due to the aluminum and titanium contents in question. These costs are to be understood throughout the program. If determined to be prohibitive, option two will be pursued at greater scale than initially proposed.

2. Pickling and *Getters*

The use of pickling and getters rely heavily on part and furnace cleanliness. Acid-pickling is a surface preparation method used to remove surface oxides. Practice at Brayton has proven successful when brazing alloys 230, 617, and 625. Alloys 230 and 625 exist close to the 0.4%Al/Ti by wt. rule with alloy 617 being an intermediate to alloys 282 and 740H. Preliminary pickling practice with Haynes 282 at Brayton has yielded unsuccessful results.
Getters are oxide sinks placed in the vacuum furnace to absorb environment oxygen and potentially strip oxides from the surface of to-be-brazed components. Note the ZrO_2 equilibrium curve in Figure 5. Zirconium has been shown to successfully enable the brazing of alloy 718[13, 23].
The combination of pickling and a Zr getter suggests that brazing alloys 282 and 740H may be possible. This approach embodies elevated risk and will be used as a secondary development path due to potential economic advantages. Some trials will be conducted but will not be held with priority unless Ni-plating becomes cost prohibitive.

Prior to brazing, fin is to be folded, plated and given a lower solution anneal temperature band heat treatment in attempt to mitigate detrimental grain growth in the thin forms. The solution anneal temperature is to be determined post assessment of the as-received material characterization solution annealed. This annealing step is to prepare the parent metal and plating microstructure for brazing diffusion [11].

Three braze alloys were initially considered: Metglas alloys MBF20, MBF50, and MBF80 (AWS BNi2, BNi5a, and BNi9 respectively) – see Table 2. Braze alloys BNi2 and BNi5a have been previously demonstrated capability of meeting sCO2 demands. BNi9 has been demonstrated with Haynes 282 and has a recommended braze temperature at the lower solution anneal temperature band, however, does not have any Silicon content, rather increased Boron content. Given prior success with BNi2 and BNi5a and the positive literature surrounding Ni-Cr-B-Si braze alloys, BNi2 and BNi5a are primary candidate alloys for this development [11, 12]. BNi5a is to be employed for fin, plate, and edge bar joining. BNi2 is to be used for secondary processes, where applicable.

Table 2: Candidate braze alloy definitions [24]

MBF Alloy	Classification	Nominal Composition, wt %						Melting Temp. °C		Braze Temp. °C
		Cr	Fe	Si	C	B	Ni	Solidus	Liquidus	
20	AWS BNi2/AMS 4777	7.00	3.00	4.50	0.06	3.20	Bal.	969	1024	1055
50	AWS BNi5a	19.00	-	7.30	0.08	1.40	Bal.	1052	1144	1170
80	AWS BNi9	15.20	-	-	0.06	4.00	Bal.	1048	1091	1120

The proposed diffusion hold braze cycle for this project is shown in Figure 6 with two different variations on the hold and temperature callouts for the braze alloys involved. The cycle temperature profile ramps to BNi5a braze temperature and then drops to the diffusion hold temperature. The intention of this hold is to alloy braze alloy melt depressants and grain boundaries to diffuse eliminating any residual eutectics at the joint interface. This is ideally conducted at the solution anneal temperature but the diffusion process and growing grains have competing objectives. With the thin form, too much grain growth results in fewer grains through the form thickness. For thin sheets, practical experience suggest between six and ten grains are desirable through the thickness for repeatable behavior but also larger grains are desirable for creep-rupture performance. For foils, as few as 2.5 grains through the thickness is potentially okay. For this reason, specification of the diffusion hold temperature is going to depend on the microstructure characteristics of the as-receive material and fin prior to the braze cycle. A diffusion hold temperature will be specified to manage the grain count through the thickness and the effectiveness of the diffusion will be a result of the specification.

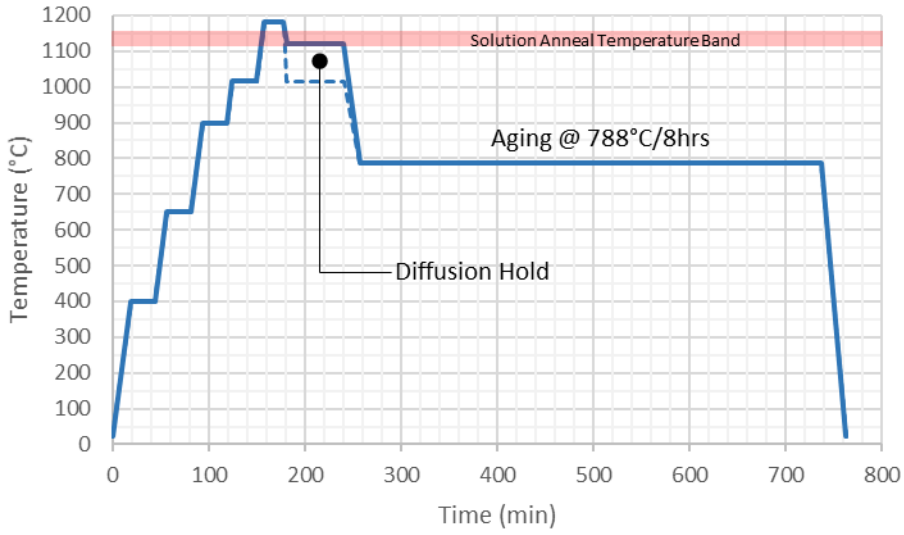

Figure 6: Diffusion hold braze cycle and single step gamma-prime precipitate aging process

Typically for Haynes 282, a two-step aging process is used. However, the use of a single step has been shown to yield similar creep-rupture behavior and therefore will be employed in this program [3]. The aging process is presented here immediately after the braze diffusion hold. The economics of this may not make sense at scale but for sake of simplicity in this program, it is included here.

Milestone 1.1.1

Table 3: Detailed Milestone 1.1.1

M #	Milestone Title	Description	Metric	Success Value	Assessment Tool	Metric Justification
1.1.1	Design-of-Experiments definition and uncertainty	Define scope of characterization using Design-of-Experiments (DoE) approach. Degrees-of-Freedom (DoF) to identify: material, sheet thickness, temperature range, stress range, strain range, sample size	Estimated Larson-Miller Parameter uncertainty based on granularity of collected data points	<10%	Uncertainty analysis considering provided DoE inputs, instruments to be used, and data with standard deviation analogous to existing sets of similar material and/or similar form factor	Typical variance of large thick-sheet and plate datasets is 1-3% deviation about trend line. Standard practice employ 95% lower-bound trend lines. Smaller datasets, particularly with thin sheet tend to be higher.
			Estimated fatigue cycles-to-failure uncertainty based on granularity of collected data points	<50%	Uncertainty analysis considering provided DoE inputs, instruments to be used, and data with standard deviation analogous to existing sets of similar material and/or similar form factor	Plus or minus 50% is a generally accepted margin for fatigue cycles-to-failure.
			Verification and validity approval of DoE inputs from independent third parties (EPRI, INL, other)	Formalized questionnaire shared with 3-5 parties of potential interest	Technical memo discussing experimental setup and value added to the technical field	Validation of technical added value from an unbiased source

- The number of test articles specified yielded uncertainty in estimated Larson-Miller Parameter: 2.5% at 100 MPa, 5.8% at 50 MPa
- Uncertainty in estimated fatigue cycles to failure, *N*, remained at (+/-)50% as this represents the best possible case for fatigue data scatter band.

- A formalized questionnaire was not disseminated, rather conversations were had with EPRI, Special Metals, Haynes, and Elgiloy. Feedback expressed concern around thin foil oxidation and high temperature integrity. But interest and concerns lack test data, validating this effort.

ii. Subtask 1.2: Material procurement

Four variations of Haynes 282 and Inconel 740 have been identified as candidate thin sheet and foil constituents for heat exchanger construction. Haynes 282 0.004” foil product was procured from Elgiloy Specialty Metals, 0.008” foil product from Ulbrich Stainless Steels and Special Metals, and 0.020” sheet from Haynes International. Inconel 740 0.018” sheet product was procured from Special Metals. The as-received condition is solution-annealed for both alloys and all forms. These described alloys and forms will be henceforth referred to as the candidate alloys or candidate forms, meaning the array of both alloy and form thickness.

Procurement of Inconel 740 proved to be a challenge and the acquisition of the six 0.018”x 24” x 36” sheets has been considered a success. Due to the limited quantity, the Inconel 740 testing campaign has been largely limited to that of Task 2 and manufacturing trials in Task 3. Attempt was made to RFQ for re-rolling sheets to thinner product form capable of producing fin but ultimately challenged by manufacturing limitations given the stock product form. ORNL has successfully conducted lab-scale re-rolling trials down to 0.010” but efforts remained unoptimized and confined to Task 2 with the limited supply.

b. Task 2: Fundamental Development

i. Subtask 2.1: Material benchmarks

This subsection describes baseline material characterization as pertains to the subsequent manufacturing and testing campaigns.

Baseline metallography of the Haynes 282 and Inconel 740 thin sheet and foil was conducted at both Oak Ridge National Laboratory (ORNL) and Sturbridge Metallurgical Services (SMS) in Sturbridge Massachusetts. Pertinent to this study is the grain size effect and the relation to creep-rupture behavior in thin product form. ORNL has developed a relation of heat treatment and grain size growth in attempt to quantify manufacturing process implications. SMS has performed some characterization of Haynes 282 and Inconel 740 in the as-received condition for all relevant product forms.

For heat exchanger construction featuring braze plate and folded fin, the brazing process presents ample opportunity for microstructural evolution in parent metals. To understand how the candidate alloys and forms are going to respond to the brazing process, a series of representative heat treatment processes were conducted. Foil samples were subject to a combination of two durations and two temperature representative of a typical Nickel alloy brazing process. Times and temperatures include

20 and 60 minutes, and 1100°C and 1150°C, respectively. Haynes 0.008” and 0.020” and Inconel 740 0.018” product form endured this heat treatment experiment. Haynes 282 0.004” was in the process of procurement during the period of performance.

Candidate brazing temperatures in Subtask 3.2 range from 1120°C-1170°C and Haynes 282 and Inconel 740 alloy solution annealing temperature bands range between 1121°C-1150°C. The proximity of brazing temperature and solution annealing temperature suggests that grain growth in the brazing process may be expected. Depending on the braze assembly, a duration as short as 20 minutes or as long as 60 minutes may be required.

Graphical heat treatment study results for Haynes 282 0.008” are shown in Figure 7. Representative grain structure is provided in the as-received condition as well as for 20 or 60 minutes at 1100°C or 1150°C for a total of five material conditions. The intercept technique was used here for grain size quantification (Figure 7d). A total of six lines were drawn per image and three images used per alloy, material form, and heat treatment condition.

Figure 8a thru c shown little to no effect of 20 or 60 minute annealing at 1100°C for all foils. The slightly lower grain size for Haynes 282 0.023” foil after 1100°C annealing is likely not related to annealing but rather foil to foil variation. The implications of raising annealing temperature to 1150°C are shown in Figure 8d thru f. The effect of annealing for 20 minutes at 1150°C varies depending on the alloy and form. The Haynes 282 0.008” and 0.023” foil shown little and no growth, respectively. The Inconel 740 foil grain size nearly doubles. The effect of annealing for 60 minutes at 1150°C shows significant grain growth for each alloy and form. Average thickness grain size measurements for each case are shown in Table 4. Reported grain sizes are an average of measurements taken along the length and through the thickness.

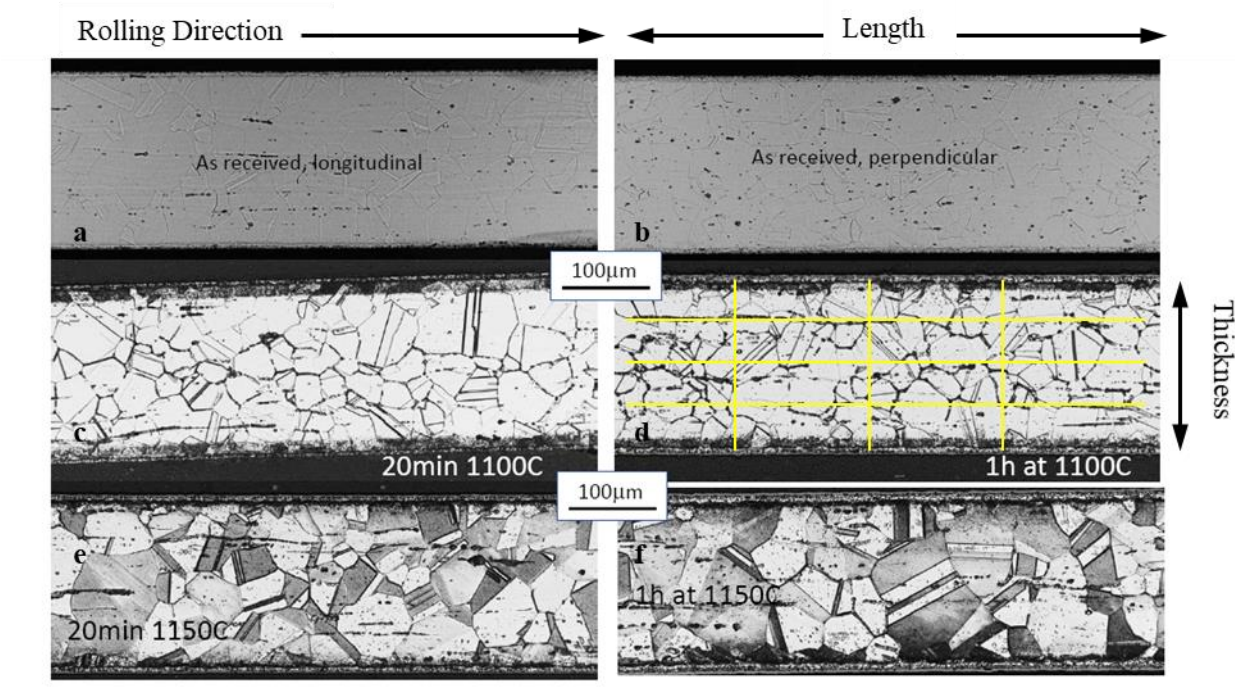

Figure 7: Haynes 282 0.008" Grain Size Characterization Graphics

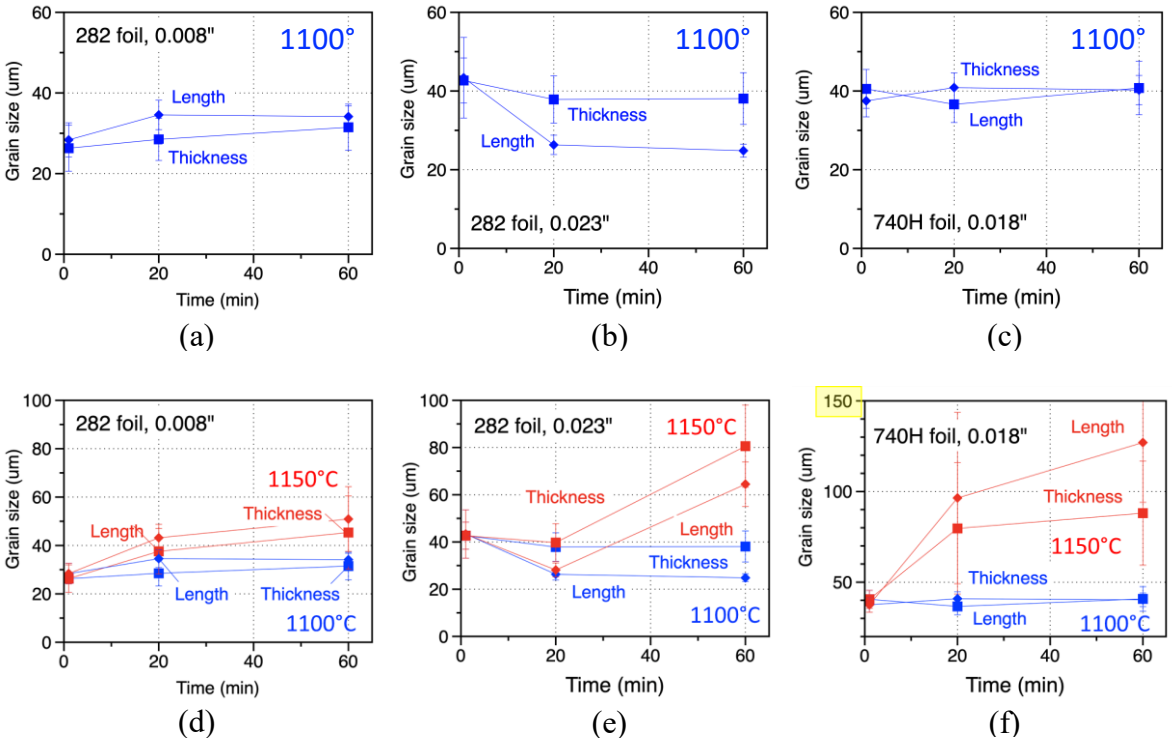

Figure 8: Grain size growth relation with time and temperature

Table 4: Grain Growth Measurements

Alloy	Form	Time	Temperature	Average Grain Size	Grain Growth		Thickness Count
		min.	°C	µm	µm	%	-
Haynes 282	0.008	As-Received		27	0	0	7.5
		20	1100	32	5	17	6.4
		60	1100	33	6	22	6.2
		20	1150	40	13	50	5
		60	1150	48	21	79	4.2
	0.023	As-Received		43	0	0	13.5
		20	1100	32	-11	-27	18.4
		60	1100	32	-11	-26	18.2
		20	1150	34	-9	-21	17.2
		60	1150	73	30	68	8
Inconel 740	0.018	As-Received		24	-19	-45	19.2
		20	1100	26	-17	-40	17.6
		60	1100	20	-23	-53	22.5
		20	1150	85	42	97	5.4
		60	1150	109	66	152	4.2

Most notable takeaways from this grain size study are the rows of Table 4 where thickness count is below six. Recall for thin sheet and foil, notionally between 2.5 and 6 to 10 grains are desired through product thickness to ensure reliability and predictable failure mechanisms. The time at 1150°C is appreciable and producing thru-wall grain counts less than practically desired. The technical implications of this are to be investigated via creep testing in attempt to quantify a currently notional understanding.

Results for Haynes 282 in the 0.008” and 0.023” product form are adequate to set bounding estimates on how 0.004” product from will behave.

Degrees of freedom in the brazing process include braze alloy, braze temperature, and time at braze temperature. Results from this study aim to inform the final brazing process parameters and supplement the Task 3 manufacturing trials.

SMS was contracted to perform a baseline alloy characterization for both Haynes 282 and Inconel 740 alloys. The characterization includes (1) alloy elemental composition, (2) grain size and texture, and (3) carbide and gamma prime precipitation. Each characterization item is included for the following product forms: Haynes 282 0.004”foil, 0.008” foil, 0.020” sheet, 0.125” sheet, and Inconel 740 0.018” sheet.

The samples were analyzed using X-Ray Fluorescence (XRF) to positively identify the material alloy. Representative pieces of each sample were sectioned, mounted, and polished per ASTM E3. Sample Inconel 740 was etched per ASTM E407 using Glyceregia (etchant #87). The remaining samples were etched per ASTM E407 using waterless Kalling’s (etchant #94). Grain size was determined on the etched samples using the comparison method per ASTM E112. Characterization conclusions included:

- Optical microscopy did not observe γ’ in any of the samples. This may be confirmed with further testing such as XRD or Electron microscopy as the γ’ phase may be too small to detect optically.

- Gray stringer inclusions with carbide-like formations were observed optically. Confirmation of the micro chemical composition may be confirmed by EDS.
- Based on the elements detectable by XRF the Seto Inconel 740- 0.018" sample was confirmed as Inconel 740 (UNS N07740)
- Based on the elements detectable by XRF the four H282 samples were confirmed as Haynes 282 (UNS N07208).

Table 5: As-received material grain size benchmark

Sample ID	ASTM Average Grain Size
Inconel 740 0.018"	6.0
H282 0.004" Foil	7.5
H282 0.008" Foil	6.0
H282 0.020"	6.0
H282 .125"	4.0

Milestone 1.2.1

Table 6: Detailed Milestone 1.2.1

M #	Milestone Title	Description	Metric	Success Value	Assessment Tool	Metric Justification
1.2.1	Baseline metal characterization	Definition of baseline characteristic material properties. Alloy composition, precipitate concentration, carbide precipitates, grain size/form, thickness tolerance, oxidation scale.	Alloy composition	Measured minimum, nominal, maximum composition values within 10% of technical literature and, if applicable, manufacturer certification and standard specification	UNS N07740, UNS N07208, ASTM B983, AMS 5951, ASTM B906	Developed standards for commercial precipitation-hardened nickel alloys require compliance to established composition and demonstration of properties. Existing standards will be used for procedure baseline when applied to new material and form.
			Grain size and texture	(+/-) 1 ASTM grain size number Percent composition of equiaxed/columnar grain structure	ASTM E 112, SEM image processing	Standard covers three basic procedures of increasing precision for estimating and rules for expressing the average grain size of metals.
			Gamma prime precipitate characterization	95% confidence interval on size and volume fraction	Comparison with literature data for thick sheets and plates	Definition of size and volume fraction is needed for performance correlation
			Thickness tolerance	<0.0002 Typ. Stdev	Micrometer measurements along axial length of stock coil. Repeated once per linear foot of fin stock. Repeated once at center and once at each end for uniaxial test specimen	Thickness specification and variance plays large role in test stress.

- Test article alloys were confirmed as the respective UNS classifications
- Test article alloy grain sizes were benchmarked. Texture notes were made and attributed mainly to the rolling direction of the materials
- No gamma prime was measured in the as-received (solution annealed) materials. Aging heat treatments were give before heat treatment.
- Micrometer measurements were taken on test articles yielding thickness tolerances accurate to within .0003-inch.

ii. Subtask 2.2: Uniaxial creep testing

A total of 14 uniaxial creep tests are summarized in *Table 7* for Haynes 282 foils. The testing included as-received plus aging performance benchmarks of the 4 mil and 8 mil foils. And additional heat treatments representative of brazing operations that the foil in the as-manufactured condition would see, temperatures include 1175°C and 1100°C, both are viable for high strength nickel alloy brazing and bound the solution annealing temperature band for Haynes 282.

Table 7: Haynes 282 uniaxial creep test results

ORNL ID	Material	Thickness (in)	Condition	Temp. (°C)		Stress (MPa)	Rupture (h)
TN39497	H282	0.008	As-Received + 4 hrs at 800°C	700	973	420	2129
TN39498	H282	0.008	As-Received + 4 hrs at 800°C	750	1023	300	2484
TN39476	H282	0.008	As-Received + 4 hrs at 800°C	800	1073	210	761
TN39663	H282	0.008	20 min at 1175°C + 4 hrs at 800°C	750	1023	385	58
TN39662	H282	0.008	20 min at 1175°C + 4 hrs at 800°C	800	1073	260	81
TN39935	H282	0.008	20 min at 1175°C + 4 hrs at 800°C	700	973	420	464
TN39936	H282	0.008	20 min at 1175°C + 4 hrs at 800°C	800	1073	210	295
TN39596	H282	0.004	As-Received + 4 hrs at 800°C	750	1023	385	58
TN40141	H282	0.004	As-Received + 4 hrs at 800°C	750	1023	235	1478
TN39595	H282	0.004	As-Received + 4 hrs at 800°C	800	1073	260	53
TN40278	H282	0.004	20 min at 1100°C + 4 hrs at 800°C	750	1023	235	1012
TN40279	H282	0.008	20 min at 1100°C + 4 hrs at 800°C	750	1023	235	724
TN40143	H282	0.008	20 min at 1100°C + 4 hrs at 800°C	800	1073	210	681
TN40277	H282	0.02	20 min at 1100°C + 4 hrs at 800°C	750	1023	300	1726

At project initiation, it was hypothesized that increasing foil heat treatment temperature would correlate to decreased creep properties and that decreasing foil thickness would also correlate decreased creep properties.

Figure 9(a) shows three test cases for 8mil Haynes 282 at 800°C, and 210 MPa, each given a different pre-test heat treatment. The data supports the theory with the as-received material demonstrating the longest rupture life and the highest heat treatment temperature demonstrating the shorted rupture life.

The test case debunking the previously defined thickness trend is the 8 mil, 750°C at 235 MPa, 20 min at 1100°C case, shown in *Figure 9*(b). Comparison of the blue and green trendlines shows that the 8-mil foil under-performs the 4-mil foil for the same conditions. While this case does make it difficult to explicitly state a clear form thickness conclusion, aggregate data trendlines to support the theory of the form thickness debits. And, depending on the confidence interval set to the trendline, there is overlap inherent in the dataset scatter.

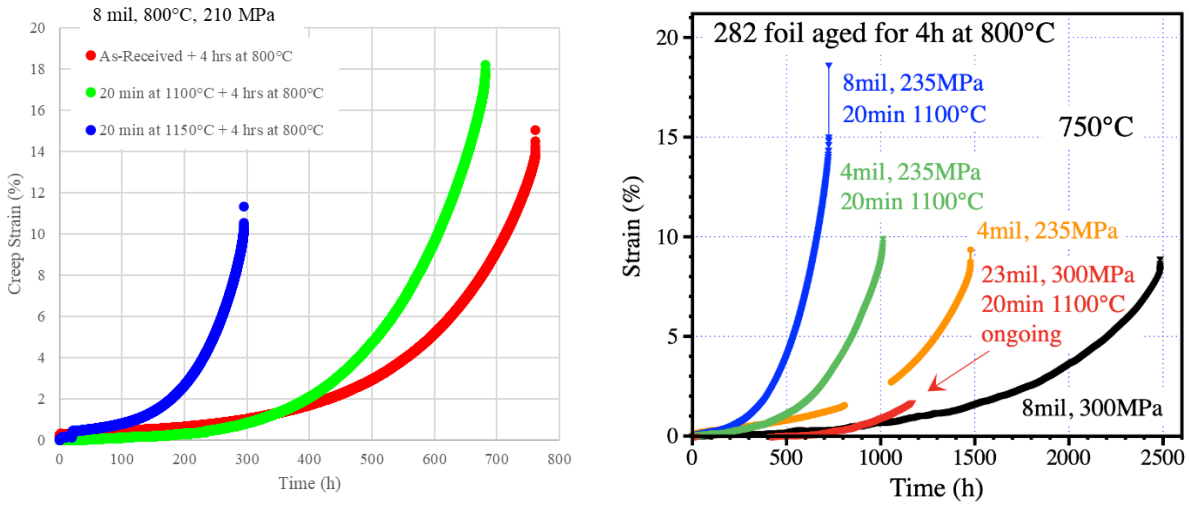

(a) (b)

Figure 9: Uniaxial test results (a) heat treatment comparison (b) form-thickness comparison

Other thoughts regarding the state of relative observations:

- Aging heat treatment is oxidizing to a potentially damaging degree. Metallography of as-received material is to be benchmarked with the test samples to determine the aging heat treatment implications. The aging heat treatment also stands to be optimized.
- This is still a limited dataset, only two tests on the 8mil foil after the 20min 1100°C anneal have been completed. Due to the limited number of grains in the tested volume, a broader dispersion of the results exists when compared to that for larger specimens. Crystal plasticity has showed that the main impact of decreasing specimen size was to increase the spread of the results. It might be realistic that these results are closely related, and scatter bands overlap.

The project-specific data compilation along with reference data and trends in the form of the Larson-Miller Parameter is provided in *Figure 10*. As a baseline, existing Haynes 282 data is shown along with a (-)3-sigma trendline for reference. The as-received 8-mil datapoints collected in this project exist well within the nominal scatter band of the thicker form trend minimal form thickness debit while the as-received 4-mil datapoints do support the form thickness debit theory. All subsequent data point with a simulated braze-cycle heat treat demonstrate a debit, favoring the (-)3-sigma trendline. In comparison with Haynes 230, plate and foil form, there is still a significant strength benefit.

For example, at 750°C and 235 MPa, nominal Haynes 230 plate ruptures in 18 hours whereas Haynes 282 4-mil foil ruptures in 500-2500 hours.
Alternatively, the 100,000-hour rupture stress at 750°C for nominal Haynes 230 plate is 72 MPa, whereas Haynes 282 foil is 113 MPa.

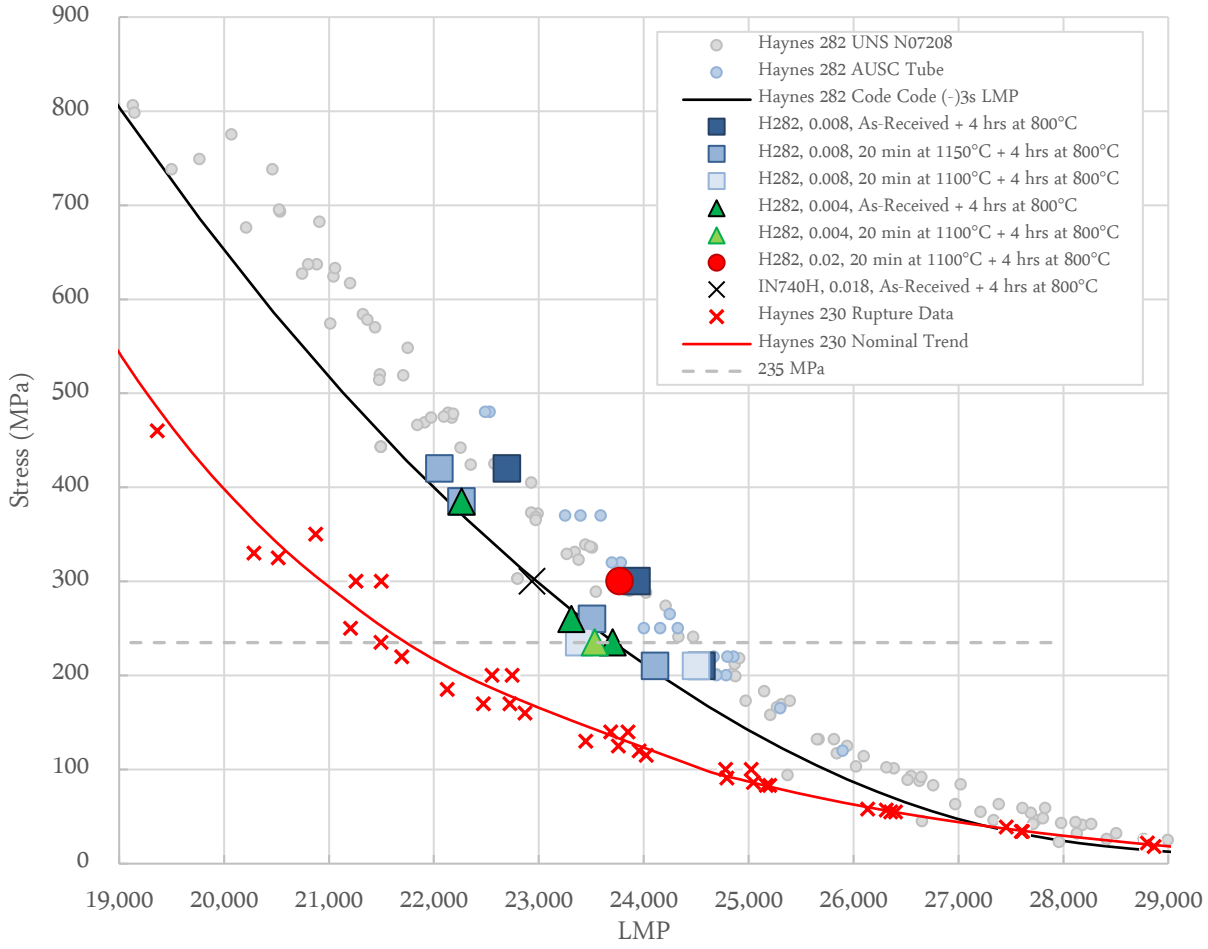

Figure 10: Larson-Miller Parameter, C = 20

Milestone 1.2.2 and 2.2.3

Table 8: Detailed Milestones 1.2.2 and 2.2.3

M #	Milestone Title	Description	Metric	Success Value	Assessment Tool	Metric Justification
1.2.2, 2.2.3	Uniaxial creep characteristics - as-received wrought materials	Construct typical and (-)3σ σ-tr and LMP. Use existing thick sheet and plate database as benchmark.	Creep-rupture LMP uncertainty	<5%	Uncertainty analysis considering variables in geometry, operating conditions, and test setup	Quantified uncertainty of critical design parameter. Typical variance of large thick-sheet and plate datasets is 1-3%
			Creep-rupture LMP standard deviation	<200 LMP	95% confidence interval based on measurement deviation from power-law trend line	Typical standard deviations of relevant large datasets exist between time-temperature values of 50 and 200

- Larson-Miller uncertainty based on time and temperature instrumentation is 50 units or approximately 0.2%
- Reported stress uncertainty based on load and cross-sectional area is 5 MPa or approximately 2.6%
- LMP standard deviation and thickness debit is summarized in Table 9.

Table 9: Haynes 282 Larson Miller Parameter by Condition

	R^2	σ (LMP Units)	2σ (LMP Units)	Debit (LMP Units)
.008”, As-Received + 4h at 800°C	0.973	55	110	121
.008”, 20min at 1175°C + 4h at 800°C	0.996	22	44	773
.004”, As-Received + 4h at 800°C	0.994	19	37	894

iii. Subtask 2.3: Failure analysis

Twelve samples were mounted and imaged. Observation commentary is as follows:

1. Carbide formation along grain boundaries make grain boundaries visible in many pictures
2. Internal oxidation/recrystallization varies based on testing conditions. Significant internal oxidation/cracking at grain boundaries at 800°C
3. As expected, larger grains are observed after 20min at 1175C
4. Comparing test conducted on the 8mil foil at 750C with (235MPa) and without (300MPa) annealing at 1100C, the annealed specimen exhibits more internal oxidation although the test duration was much shorter. The grain size seems also larger or fewer GB are decorated with carbides
5. The 740H specimen was machined perpendicular to the rolling direction (cannot see aligned carbides like in the 282 micrographs). Fracture surface is quite different with the presence of many voids/cracks at grain boundaries

A representative example graphic is shown in Figure 11.

No notable observations were recording invalidating any of the obtained data. And no notable observations were able to quantify the relationships observed with form thickness or heat treatment. However, a good optical dataset was created for future reference.

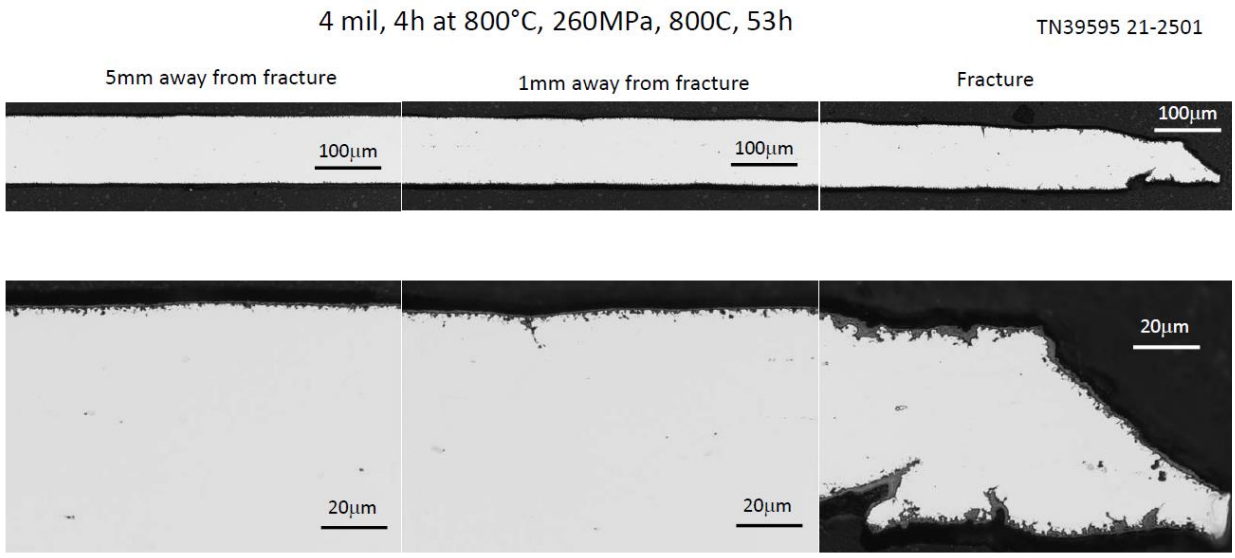

Figure 11: Optical failure analysis graphics

iv. Subtask 2.4: Material modeling

The goal of Subtask 2.4 was to create a material model with the ability to capture the creep-rupture performance implications of the theorized form-thickness debit. A continuum damage mechanics (CDM) approach was employed to capture the relevant damage mechanisms as the foils are exposed to temperature and are stressed. The material model and governing creep rate equation is outlined in Figure 12. The creep model was first created leveraging Haynes 282 code case characterization efforts and then exercised with the generated dataset. Approximately 15% of the code case dataset was used to estimate the model parameters $\dot{\varepsilon_0}$, σ_0, C, h′ and H^*

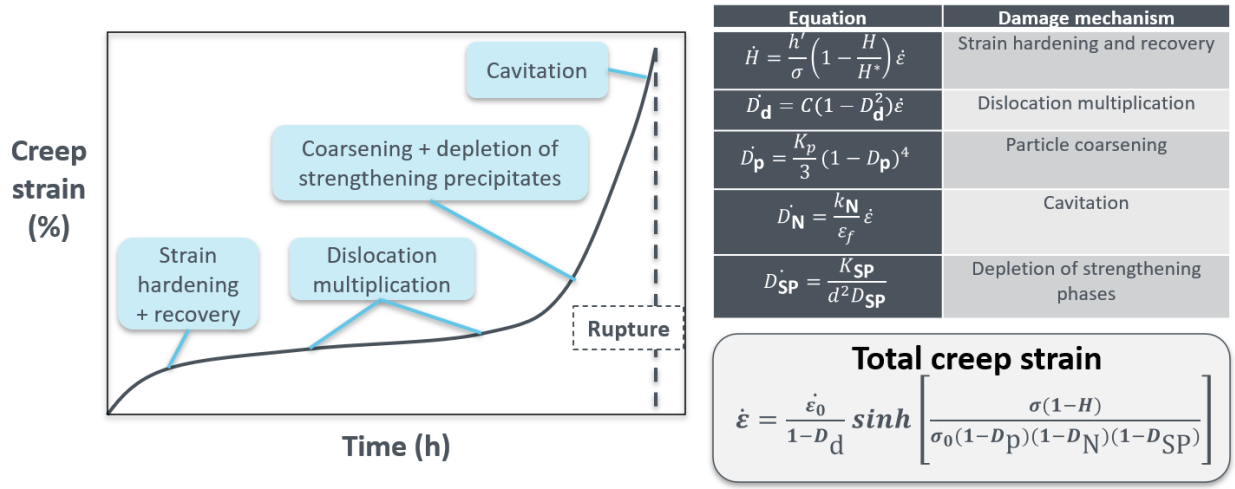

Figure 12: Physics-based CDM creep model overview

Calculated times to 2% creep strains are within 500h of measured values, meaning less than 15% variance for all tests with duration greater than 3,333 hours. And data at 704 °C was not considered for model development. *Figure 13* shows good agreement between measured and calculated values at all temperatures at which data was collected, suggesting all relevant damage mechanisms have been captured in the material model and agreement at 704 °C demonstrates the extrapolative capability of this physics-based creep model

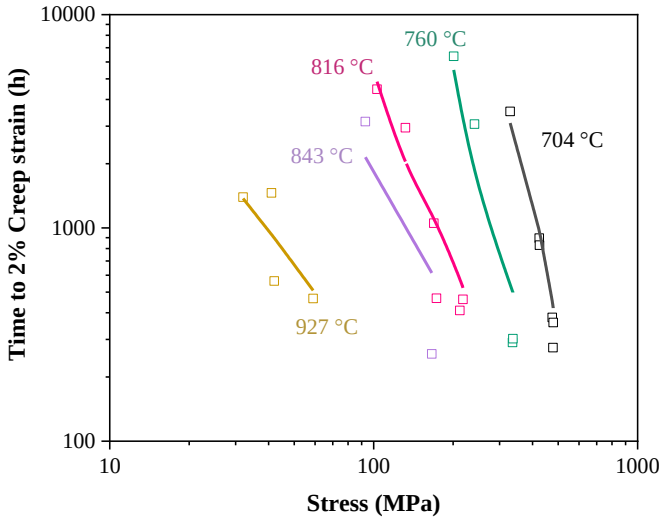

Figure 13: Creep model comparison with creep strain data

Data collection for this modeling effort yielded observation of correlation between the LMP and the temperature dependence of the volume fraction of g', $\varphi_{\gamma'}$, ($0.93 < R^2 < 0.98$), according to equation 1. A graphic from the data collection process is shown in *Figure 14*(a) and the LMP and gamma prime correlation in *Figure 14* (b). Note that the observance of the gamma-prime depletion zone is relatively small in this rather thick sample. And that the depletion zone becomes increasingly relevant with thinner forms.

$$LMP = a + b\log(\varphi_{\gamma'}) + c\log(\varphi_{\gamma'})^2 + d\log(\varphi_{\gamma'})^3 \quad (1)$$

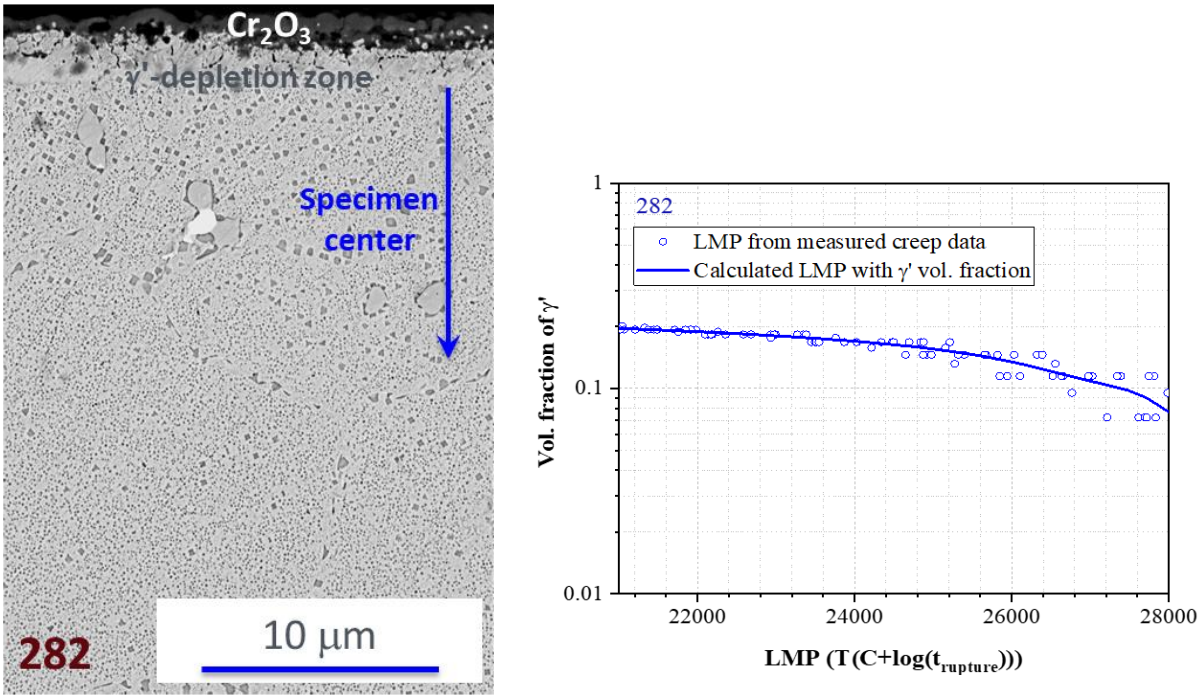

(a) (b)

Figure 14: (a) Characteristic Haynes 282 oxidation and γ' depletion (b) LMP correlation with γ' volume fraction

The LMP and gamma-prime correlation is an important observation as the depletion of the gamma prime strengthening phase is the key contributor to the theorized form thickness.

The theory and model is exercised (Figure 15) using Haynes 282 at 800°C and 210 MPa in the as-received condition. Data is presented as rupture as a function of form thickness at these conditions. A data point collected in subtask 2.2 is plotted alongside the nominal Larson-Miller parameter (+/-)1-sigma and the model nominal trend. The data point is shown existing within the 1-sigma scatter band and the model trendline pierces the nominal Larson-Miller point. At 800°C, gamma-prime depletion through the thinner-form thicknesses is driving the rupture debit.

Replication of these results with other data points draw similar conclusions and look like the Larson-Miller parameter figure.

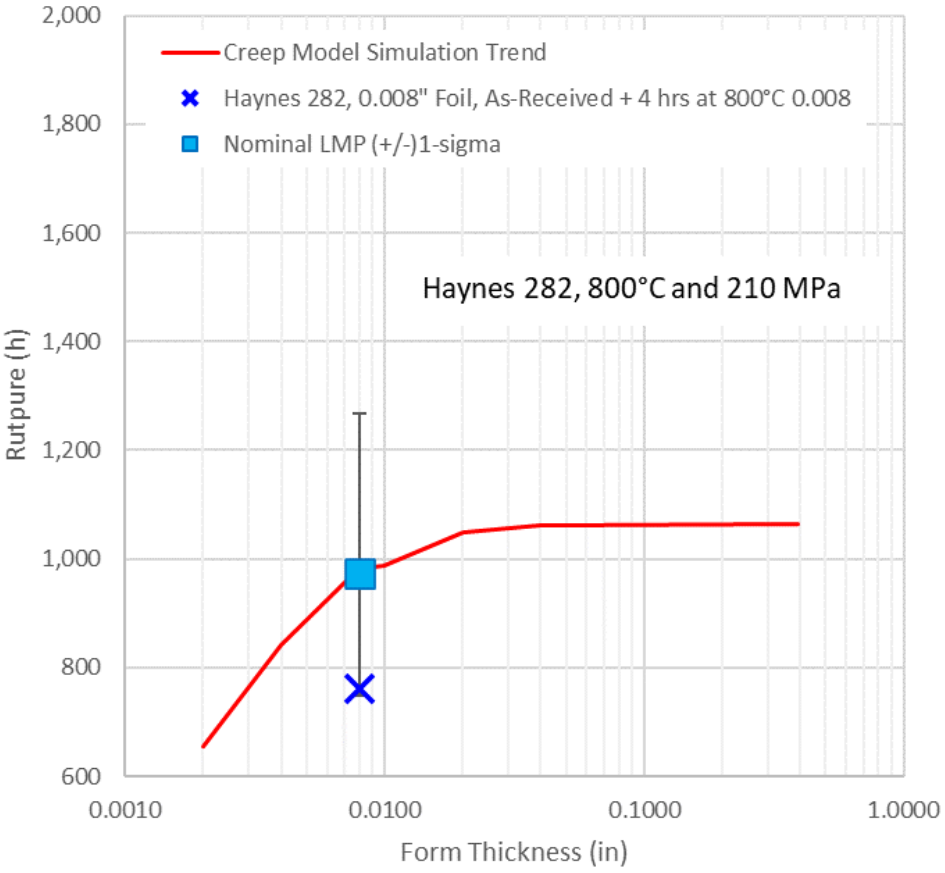

Figure 15: Creep, oxidation, and corrosion modeling results

The physics-based CDM model discussed has been incorporated into an open-source tool, it may be referenced here: https://doi.org/10.11578/dc.20220328.1

Milestone 2.2.4

Table 10: Detailed Milestones 2.2.4 and 2.2.5

M #	Milestone Title	Description	Metric	Success Value	Assessment Tool	Metric Justification
2.2.4	Uniaxial creep modeling	Leverage new and existing data to develop oxidation and corrosion models of specified materials in relevant form factors. Develop correlation of creep-rupture behavior and characteristic material properties, typical oxidation scale thicknesses, and oxidation-affected zones	Form thickness debit uncertainty from thick sheet and plate datasets	<15%	95% confidence interval on departure from thick sheet and plate behavior. Validate ORNL oxidation models with new experimental data not used to determine model parameters.	Departure in performance is expected as oxidation and oxidation-affected zones play larger role with thin form factor. Ability to predict debit is necessary design consideration.
2.2.5	Physics-Based Failure Prediction	Given a thin foil thickness (0.004"-0.023"), modeling efforts shall investigate how grain size affects the creep behavior and why there exists a magical number of grains-through-the-thickness instead of larger grains being better in thin form.	Comparison short term creep-rupture data with creep-plasticity model	50% difference in measured failure and predicted failure	Modification of existing ORNL creep-plasticity models and uniaxial creep rupture data	The goal of this milestone is to predict failure based on physical phenomenon. The model prediction will only be useful moving forward if results are similar to experimental datasets. Provided model and data agreement, the model may adjust inputs like time and temperature for extrapolation into the design space. Current literature for a Titanium alloy supports the success value used here. (Ref. https://doi.org/10.1007/s11661-006-0082-2)

- Calculated times to 2% creep strains are within 500h of measured values, meaning less than 15% variance for all tests with duration greater than 3,333 hours.
- Creep plasticity modeling results were not explicitly used, rather the correlation with gamma-prime depletion was sufficient to determine the form thickness debit using a physics-based modeling approach. Nominal modeling results agree with the 1-sigma scatter band of the larger database.

c. Task 3: Practical development

i. Subtask 3.1: Test article design

The core Task 3 test article architecture is drawn in *Figure 16*. Featured is a 4.125-inch width by 0.167-inch height by 4.063-inch length folded fin and brazed plate heat exchanger geometry. The geometry shown is representative supercritical CO2 primary heat exchangers and recuperators at smaller scale. Manufacturing test articles at this size is a common first of kind trial that allows for quick and economical iteration on manufacturing process parameters. A total of three fin configurations were made, all at the 0.124-inch height:

- .004-inch compacted round-crest by 55 fins per inch
- .008-inch round crest by 35 fins per inch
- .004-inch flat crest by 8 fins per inch

Graphics of the as-manufactured test articles (without headers) are shown in *Figure 16*.

Figure 16: Folded fin test article figures (top) drawing detail (center) flat-crest fin (bottom) round crest fin

ii. Subtask 3.2: Manufacturing process benchmarks

Manufacturing a brazed plate and folded fin heat exchanger architecture with Haynes 282 and Inconel 740 will be a first-of-kind venture. This section aims to build and quantify manufacturing process parameters using simple lap joints.

Lap-Joint Brazing and Tensile Testing

Challenge: Titanium and Aluminum oxides inhibit wetting of molten braze filler metal and the formation of robust metallurgical bonds in vacuum brazing processes typically employed for Ni-based materials.

Goal: Determine the brazing method most suitable for joining Haynes 282 and Inconel 740H. Most suitable here meaning the most economical method meeting strength and ductility requirements for a given application.

Approach: Manufacture brazed lap joints and perform tensile tests in accordance with standard practice and the ASME Boiler and Pressure Vessel Code. After a series of lap joint and tensile tests, a manufacturing process down select will be made prior to brazing any plate and fin test articles. Focus will be given to Haynes 282 because of material availability.

ASME Boiler and Pressure Vessel Code Section IX, Part QB Subsection 140 describes tests used in brazing procedure and performance qualification. Brazed lap joint tension tests will be used in this manufacturing development as a method for tensile strength and ductility quantification comparison between multiple brazing process variations. Definition for brazed lap joint test specimen is provided in Figure QB-462.1(c). The demonstrated tensile strength must be equal to, or greater than the specified minimum tensile strength per Table QW/QB-422, in the annealed condition, to pass the tension test. Unfortunately, minimum tensile strength values for Haynes 282 are not yet available in the Section IX of the Code. Alternatively, tensile test measurements on a control sample of the as-received stock will therefore be used.
Manufacturing steps for brazed lap-joint construction are shown in Figure 17 (Brayton Energy LLC part number SE80106). First, two 0.020” sheets are brazed in the lap joint configuration (SE80106-1). Tensile specimen (SE80106-2) are then waterjet cut from SE80106-1 in accordance to Figure QB-462.1(c) dimensions.

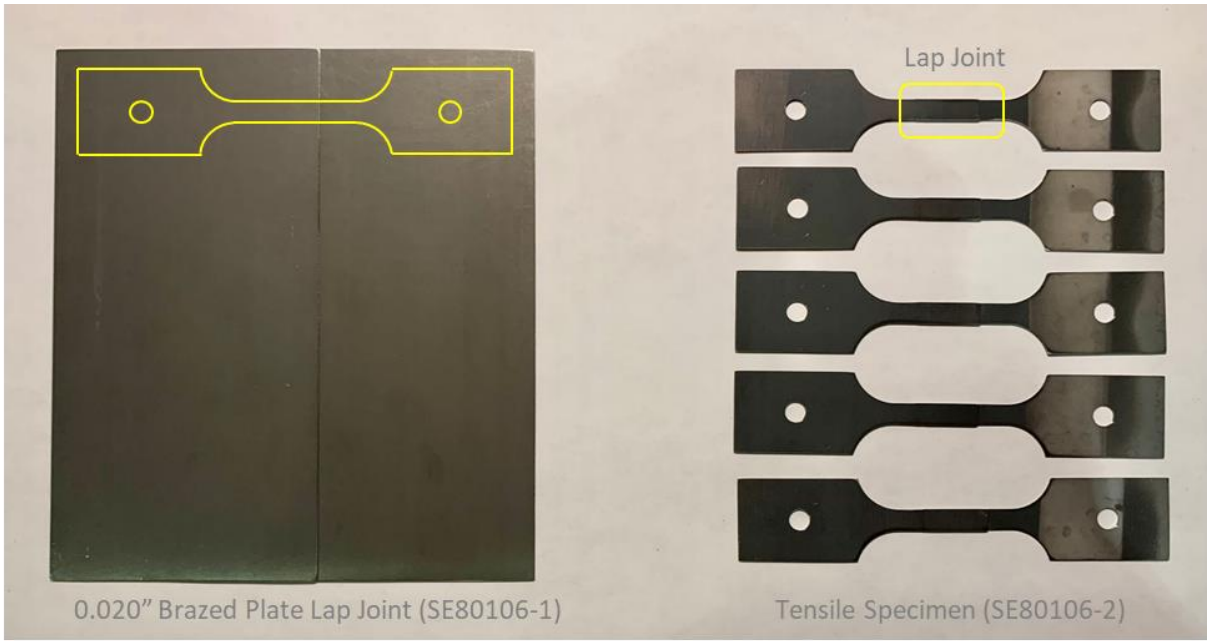

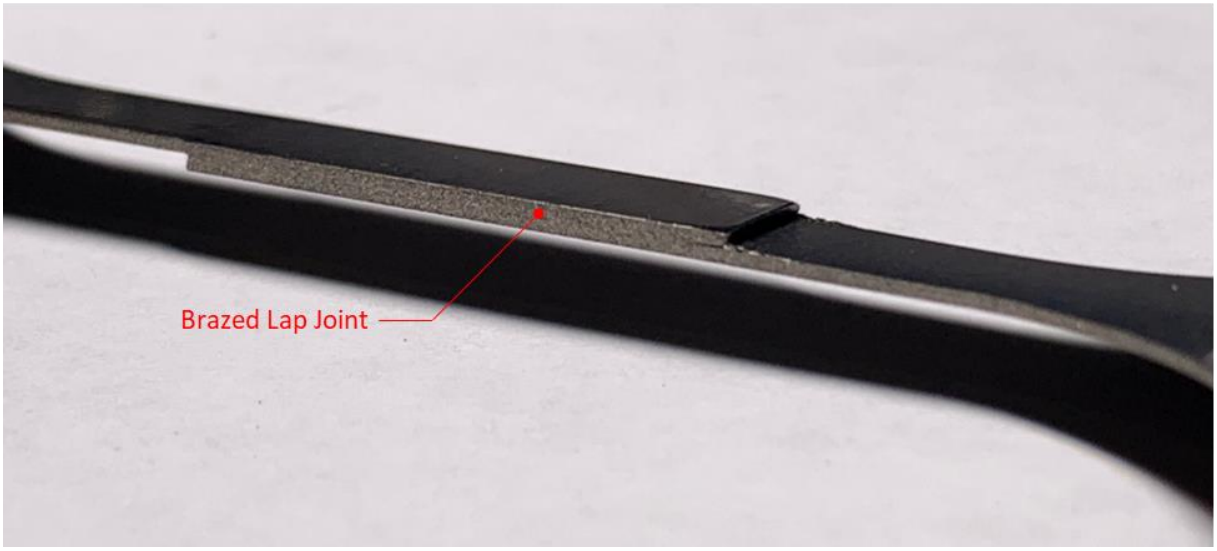

Figure 17: Braze Lap Joint Construction

Methods

The candidate surface preparation and brazing techniques are shown in Table 11, brief descriptions are as follows:

1. Standard Cleaning (SC): First, application of an aqueous degreaser for removal of tooling oils, followed by application of isopropyl alcohol for a clean surface.
2. SC + Pickle: Application of *Wonder Gel* for surface oxide removal.
3. *SC + Pickle + Zr Getter*: Zirconium exhibits a higher free energy of oxide formation relative to titanium and aluminum. Acting as an oxygen sink in the vacuum furnace, Zirconium should absorb oxygen present in the furnace environment and potentially strip oxygen from nickel surface. The furnace configuration for this approach is shown in Figure 18.
4. Melt-Point Depressant: The underlying principle of melt depressant brazing is understood as locally lowering the melting temperature such that compressive and/or surface tension forces between neighboring substrates at liquidus enable joining.
5. SC + Electrolytic Ni-Plating: Nickel plating removes the concerning presence of Titanium and Aluminum oxides at the brazed joint substrate interfaces at the expense of processing cost. Market costs and technical feasibility are to be assessed and pursued.

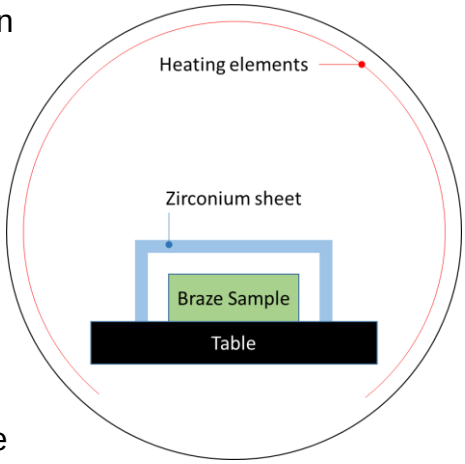

Figure 18: Ideal furnace setup with Zirconium getter

Table 11: Brazed Lap Joint Brazing Methods

Index		Surface Preparation	Braze	
			Alloy	Profile
1	A	Standard Cleaning (SC)	MBF50	1
1	B	Standard Cleaning (SC)	MBF80	9
1	C	Standard Cleaning (SC)	MBF91	10
2	A	SC + Pickle	MBF50	1
2	B	SC + Pickle	MBF80	9
2	C	SC + Pickle	MBF91	10
3	A	SC + Pickle + Zr Getter	MBF50	1
3	B	SC + Pickle + Zr Getter	MBF80	9
3	C	SC + Pickle + Zr Getter	MBF91	10
4	A	Melt Depressant	BNi2-B	4
4	B	Melt Depressant	BNi2-B	5
4	C	Melt Depressant	BNi5a-B	7
4	D	Melt Depressant	BNi5a-B	1
5	A	SC + Electrolytic Ni-Plating	MBF50	1
5	B	SC + Electrolytic Ni-Plating	MBF80	9
5	C	SC + Electrolytic Ni-Plating	MBF91	10

Melt-Point Depressants aside, each of these techniques are coupled with a Metglas amorphous brazing foil and a corresponding braze profile as outlined in the table. Metglas MBF50, MBF80, and MBF91 are brazed at their recommended temperature in a diffusion hold process post excursion to brazing temperature.
For each table line item, three tensile pull tests were (are being) completed to characterize tensile strength and elongation.

Results

Tensile loading results for the cases outlined in Table 11 are shown in Figure 19. Nominal bar values are indicative of the average value for the three samples in each category. Error bar values are indicative of the value range for the three samples in each category. As of March 9, 2021, test results for melt-point depressant cases 4A thru 4D are pending.

Four Haynes 282 cases are considered as baseline metrics for comparison of tensile load and strength results, these cases will be referenced in parallel to those outlined in Table 11 with an index of 0 and a grouping description of “Parent Material”. These cases are as follows:

- **0A, Literature (Annealed):** a manufacturer provided value with be used for tensile strength quantification [1]
- **0B: As-Received (Annealed):** a monolithic tensile specimen cut from parent material in accordance with ASME BPVC Section IX Figure QB-462.1(c) dimensions.
- **0C: Literature (Soln. Anneal + Age):** a manufacturer provided value with be used for tensile strength quantification [1]
- **0D: Braze Cycle Heat Treat:** a monolithic tensile specimen cut from parent material in accordance with Figure QB-462.1(c) dimensions subject to braze cycle profile number 1.

ASME code states that braze joint tensile strength is to be greater than minimum tensile strength. The definition of minimum tensile strength as pertains to this study is that the lap joint specimen should not fail in the lap region. Case 0D, Braze Cycle heat Treatment will be considered for the baseline tensile strength measurement.

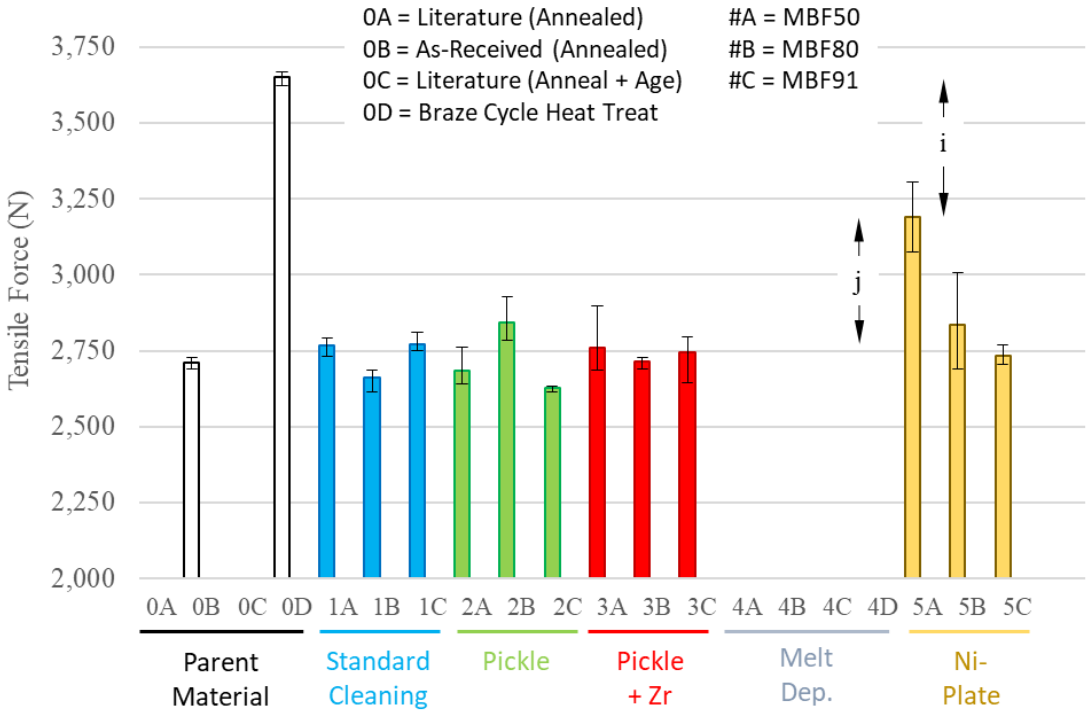

Figure 19: Tensile Testing Tensile Force Results

Figure 19 annotation *arrow i*: Case 5A represents the lap joint manufactured with electrolytic Ni-plated sheet and MBF50, meaning implications of Titanium and Aluminum oxides have been removed from the manufacturing process. Therefore, *arrow i* is indicative of the geometric difference between the monolithic and lap-joint specimen.

Figure 19 annotation *arrow j*: Cases 1A thru 3C represent lap joints manufactured with cleaned and pickled sheet, meaning Titanium and Aluminum surface oxides have been reduced prior to brazing but nevertheless present. Therefore, *arrow j* is indicative of the debit due to brazing surface preparation and process parameters.
To remove data noise associated with geometric-bias as indicated by *arrow i,* two finite element analysis (FEA) models were created for each geometry type using the material properties acquired from baseline Case 0D and the Ramberg-Osgood equation. Tensile simulation results for the monolithic and lap joint specimen are presented in Figure 20. Note that the monolithic specimen is producing peak stress in the gauge section and that the lap-joint specimen is producing slightly abnormal stress profiles because of the sheet offset with peak stresses at thickness discontinuity.

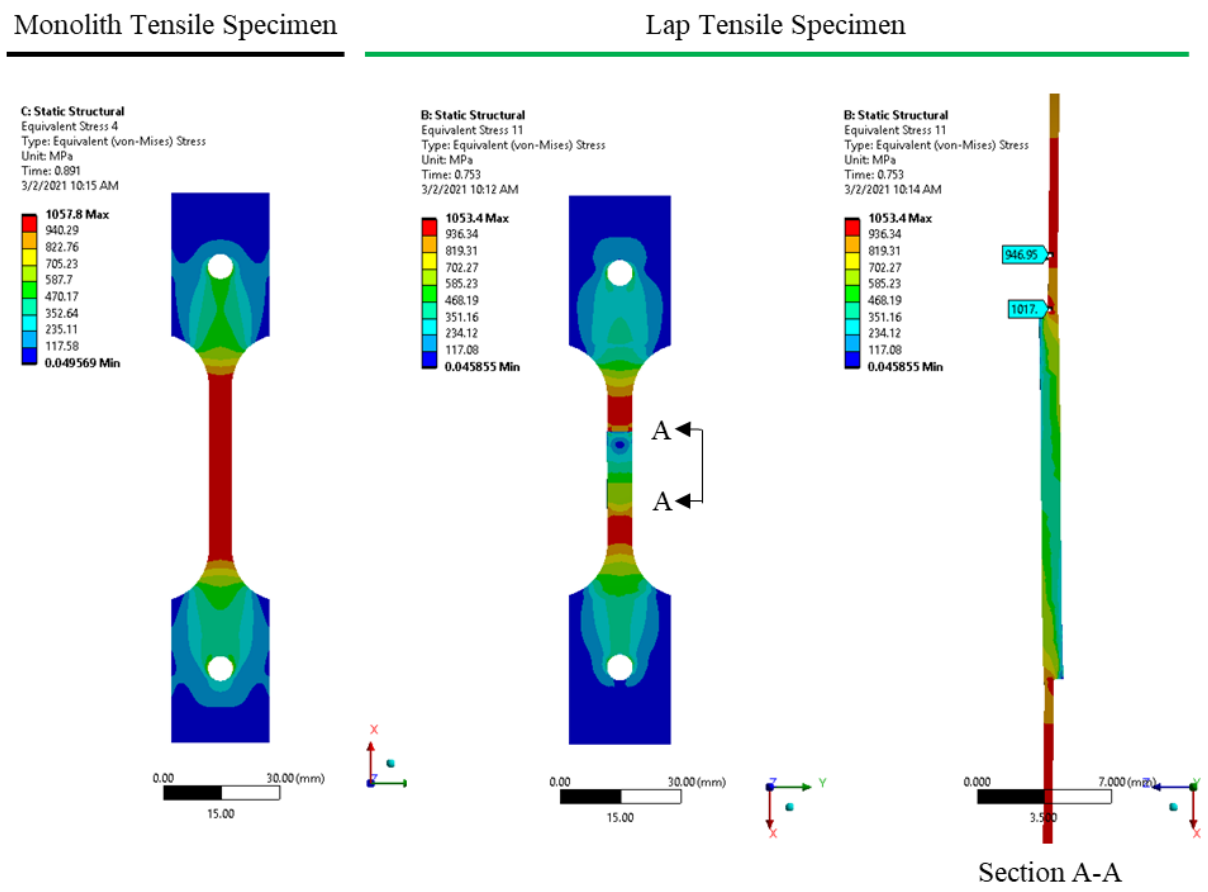

Figure 20: Tensile Testing Simulation (Monolith versus Lap)

Strain and stress results as a function of tensile load for the monolith and lap-joint specimen are shown in Figure 21 along with the data points collected in this study. As a sanity check, simulation and data for Case 0D stress at failure match. Notably, the stress and strain trendlines for the lap-joint specimen require smaller loads to replicate the same stress and strain intensities apparent in the monolith specimen, as a result of the more complicated loading. For translation of the Figure 19 data from tensile load to tensile strength, these simulation curves are used. The normalized tensile strength results are shown in Figure 22. Note that similar trend to Figure 19 is observed with the removal of *arrow i* discrepancy; Case 5A showing 97% nominal performance potential.

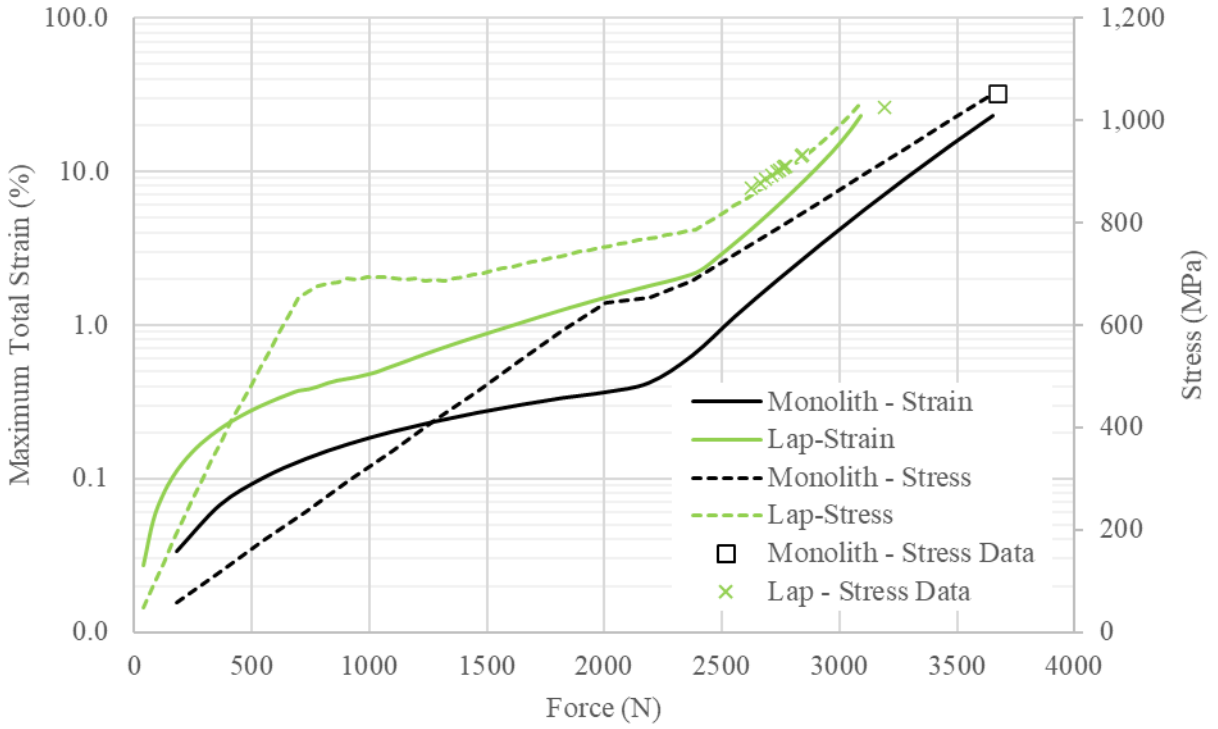

Figure 21: Monolith and Lap-Joint simulation stress and strain as a function of tensile load

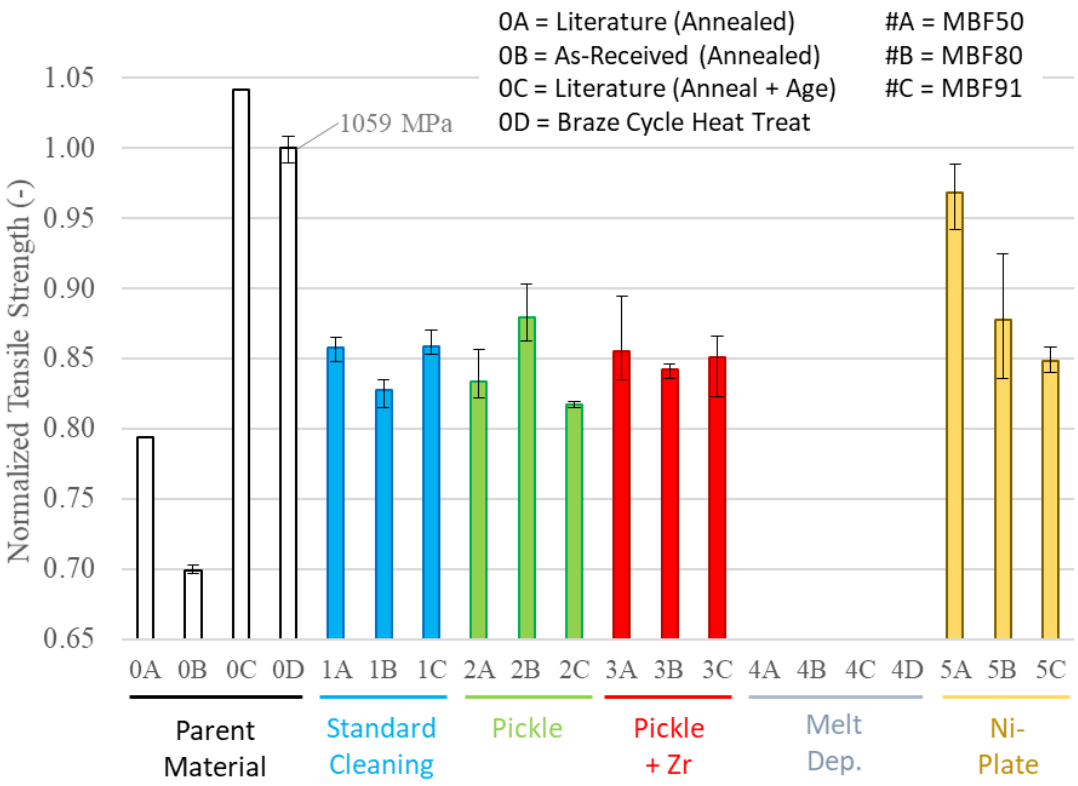

Figure 22: Normalized tensile strength figures for each brazing surface prep. technique.

Case 0B, As-Received tensile strength is 12% lower than 0A, literature values, with comparable elongation. This observed tensile strength discrepancy is likely due to heat-to-heat variation, and the thin 0D form factor, i.e., 0.020inch sheet, and is not a concern for this study but rather a benchmark.

As Case 0D, Braze Cycle Heat Treat is representative of the processing endured by cases 1A thru 5C, Case 0D is the normalizing benchmark.

Measured Case 0D tensile strength is approximately 4% less than manufacturer literature. This is viewed as within acceptable range.

Cases 1A thru 3C may be broken down into two groupings: (1) braze alloy and (2) surface preparation technique. Considered as an ancillary grouping are the Electrolytic Ni-Plated, 5A-5C cases. The average tensile strength values for each of these groupings are shown in Table 12, where darker formatting highlights greater values. MBF50 and the standard cleaning plus zirconium process parameters provides the highest on-average tensile strength, inferior to only that of the Ni-Plated grouping.

The variation between Case 5A, 5B, and 5C is attributed to the braze alloy used and the corresponding brazing temperature. Case 5A employs Metglas® MBF50 with a

Table 12: Subset Grouping Performance

Subset Grouping	Average Tensile Strength
	MPa
MBF50	837
MBF80	815
MBF91	797
SC	794
SC + Pickle	785
SC + Zr	817
ENiP	869

brazing temperature of 1170°C whereas Case 5A and 5C alloy compositions are different and brazing temperatures are lower (1120°C and 1140°C respectively).

Failure Modes

Two types of failure modes are evident with the described tensile specimen:

1. Failure Mode 1
    - Failure at edge of brazed lap joint, transition between lap and sheet
    - Shown in Figure 23 a.1 and Figure 23 a.2
    - Representative of approximately 54% of samples (as of 02/17/2021)
2. Failure Mode 2
    - Failure in parent metal between 10% and 25% of lap joint termination
    - Shown in Figure 23 b.1, b.2, and b.3
    - Representative of approximately 46% of samples (as of 02/17/2021)

Figure 23 graphics are representative of standard cleaning surface preparation and MBF50 braze foil.

In most cases, (Case 1A for example), two samples failed via mode 1 and one sample via mode 2. This is consistent across other cases (with variability) suggesting that regardless of failure mode, the reported tensile strength and elongation is accurate within the ranges shown.

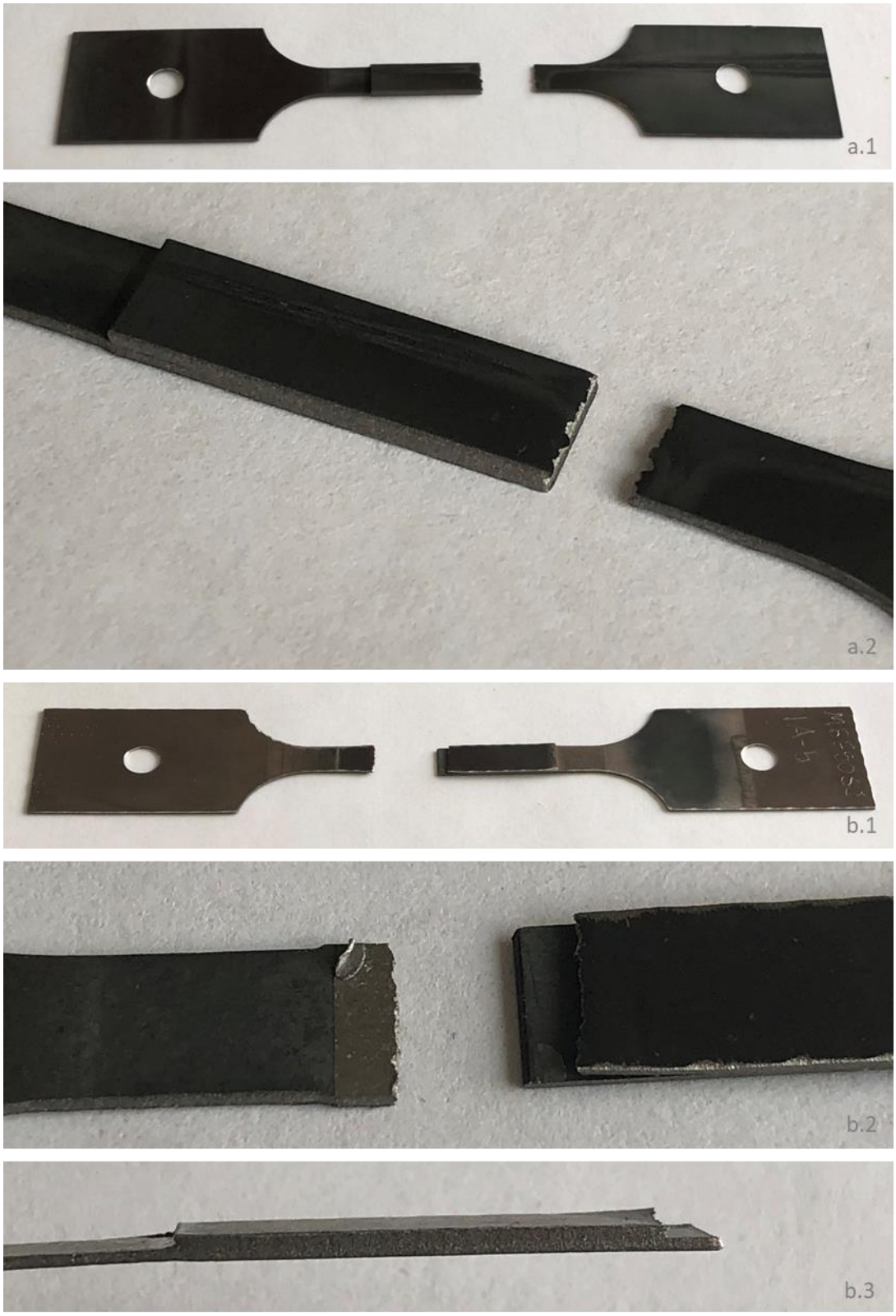

Figure 23: Brazed Lap Joint Failure Tensile Modes

Haynes 282 brazed lap joints have been manufactured in accordance with a test matrix including variations on surface preparation and amorphous braze foils used. Tensile tests on control samples and brazed lap joints have been completed and results are presented. Nickel-plated samples vacuum furnace brazed using Metglas® MBF50 filler metal yield average tensile strengths within the uncertainty range of the control case. Samples employing standard cleaning, pickling, and Zirconium Getters in lieu of nickel-plating yield average tensile strengths 16% less than control. ASME BPVC Section IX minimum tensile strength values are not yet published for Haynes 282 but solid-solution strengthened alloys show minimum tensile strengths 10-20% less than nominal. In all cases, lap-joint integrity is maintained and failure is observed in parent material suggesting a validated manufacturing process. Performance results favor the Ni-plated samples but due to the costs associated with the added processing at scale, the path forward from this study contains the following parallel efforts to understand the economic and technical aspects of these described joining methods.

1. **SC + Pickle + MBF50 + Zirconium *Getters***
   On average, cases including MBF and/or Zr *Getters* demonstrate greater tensile strength and elongation. The addition of pickling shows marginal influence on strength and ductility but is included here to replicate Case 3 results. The path forward should leverage this approach as the primary candidate for folded fin and brazed plate.
2. **Ni-Plating + MBF50**
   This combination represents the highest performing case but will likely be economically challenged. The path forward should leverage this approach in small quantity to gauge both the economics and technical viability. Ni-Plated components should include fin and plate.

iii. Subtask 3.3: Test article fabrication

The test article manufacturing process has been finely tuned and has yielded a 100% pass rate (9 of 9) for the final three batches and 88% pass rate (14 of 16) for the last four batches. A complete test article manufacturing time-history is shown in *Figure 24*. A near linear increase in yield rate trend is observed between March and September, plateauing at 100% since. As of this reporting period, the manufacturing process is considered fully developed.

A total of 36 samples have been manufactured to date, with 18 qualifying as test articles. The test matrix requires no new samples required to be manufactured, pending the success of outstanding tests. The final creep tests are on pace to begin in February 2022. Most outstanding fatigue tests are on pace to begin in February 2022 with a few extending to March 2022.

Each sample is hydrostatically charged at two stages, first after brazing the plate and fin and then after brazing headers. The first hydro test is only a few hundred psig, enough to justify continuing to add value. The second hydro test is in accordance to the American Society of Mechanical Engineers (ASME) Boiler and Pressure Vessel Code (BPVC) Section VIII, Division I, UG-101. Passing these hydrostatic tests, in the context of this program, constitutes a qualified test article.

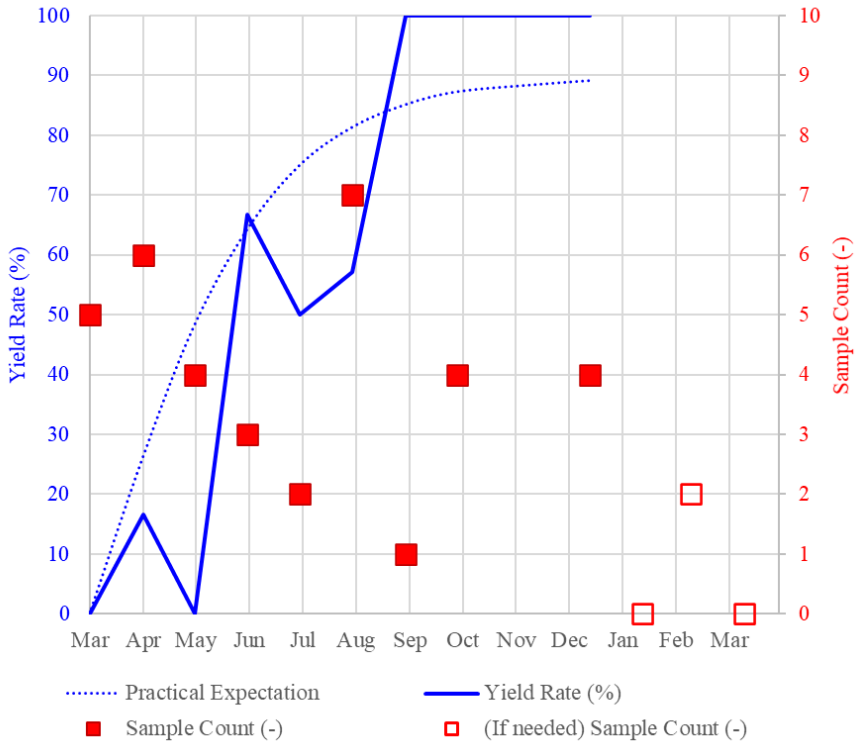

Figure 24: Test article manufacturing time history

Figure 25: Ready to service test articles

iv. Subtask 3.4 Pressurized creep testing

Pressurized creep testing consists of subjecting the Subtask 3.1 test articles to an elevated temperature environment, charging them to a specified pressure, then holding until rupture. The test measurements include a time-history of pressure and temperature. The measured time to failure is then compared with the simulated time to failure. In this section, first the method by which simulated time is determined is discussed. Then a summary of tests completed is provided and measurements are compared with what was anticipated.

A few different attempts were made at simulating creep-rupture failure of the pressurize creep tests. First, an elastic Larson-Miller and a Norton secondary creep law were used. Both approaches require significant assumptions to be made about the implications of tertiary creep. This is problematic because tertiary creep accounts for 30-70% of creep life. In this reporting period, a new modeling approach was crafted and implemented within the ANSYS finite-element framework to simulate both secondary and tertiary creep regimes. The newly proposed Haynes 282 creep model is a Continuum Damage Mechanics, or CDM-based, hyperbolic-sine creep law (or just Sinh creep law as pertains to this conversation). CDM-based modeling in this context leverages a time, temperature and stress dependent parameter that tracks accumulated (creep) damage from beginning of service, damage = 0, to failure, damage = 1. A full literature review will not be provided here but these concepts are well-founded and shown to be valid for both stainless steels and high nickel-based alloys [26, 26].

The proposed Sinh creep law is shown in equation (1), and constituent equations in (2), (3), and (4). Nomenclature for various terms and term groups is provided in Table 13. Temperature dependent coefficients (ANSYS inputs) are provided in Table 14.

This Sinh model is a secondary and tertiary creep model. The secondary creep rate is governed by the McVetty term group, and the tertiary creep rate is governed by the exponential damage-parameter term group. The advantages of this model are that both secondary and tertiary creep regimes are captured (the largest fraction of creep life) and implementation is numerically stable. A few disadvantages include the data requirements, substantial engineering development requirements, and neglect of primary creep.

$$\dot{\varepsilon}_{cr} = A\sinh\left(\frac{\sigma}{\sigma_s}\right)\exp(\lambda\omega^p) \tag{1}$$

$$\dot{\omega} = \frac{M}{\phi}[1-\exp(-\phi)]\sinh\left(\frac{\sigma}{\sigma_t}\right)^{\chi}\exp(\phi\omega) \tag{2}$$

$$M = \left[t_r\sinh\left(\frac{\sigma}{\sigma_t}\right)^{\chi}\right]^{-1} \tag{3}$$

$$\lambda = \ln\left(\frac{\dot{\varepsilon}_f}{\dot{\varepsilon}_{min}}\right) \tag{4}$$

Table 13: Sinh creep law nomenclature

$\dot{\varepsilon}_{cr}$	Creep rate (%/hr)
$\text{Asinh}\left(\frac{\sigma}{\sigma_s}\right)$	McVetty secondary creep term group
ω	Damage parameter (-)
$\exp(\lambda\omega^p)$	Exponential damage-parameter tertiary creep term group
$\dot{\varepsilon}_{min}$	Minimum creep rate
$\dot{\varepsilon}_f$	Final creep rate

Table 14: Sinh creep law constants

A	%/hr
σ_s	MPa
λ	-
M	1/hr
σ_t	MPa
ϕ	-
$p = 1.5$	constant (-)
$\chi = 2$	constant (-)

The three previously described modeling approaches are shown in Figure 26. All models show good agreement up to tertiary onset but only the Sinh creep model is capable of tracking tertiary creep. Uncertainty bars on the dataset are representative of 1-sigma Larson-Miller deviation and the typical range of creep strain at failure.

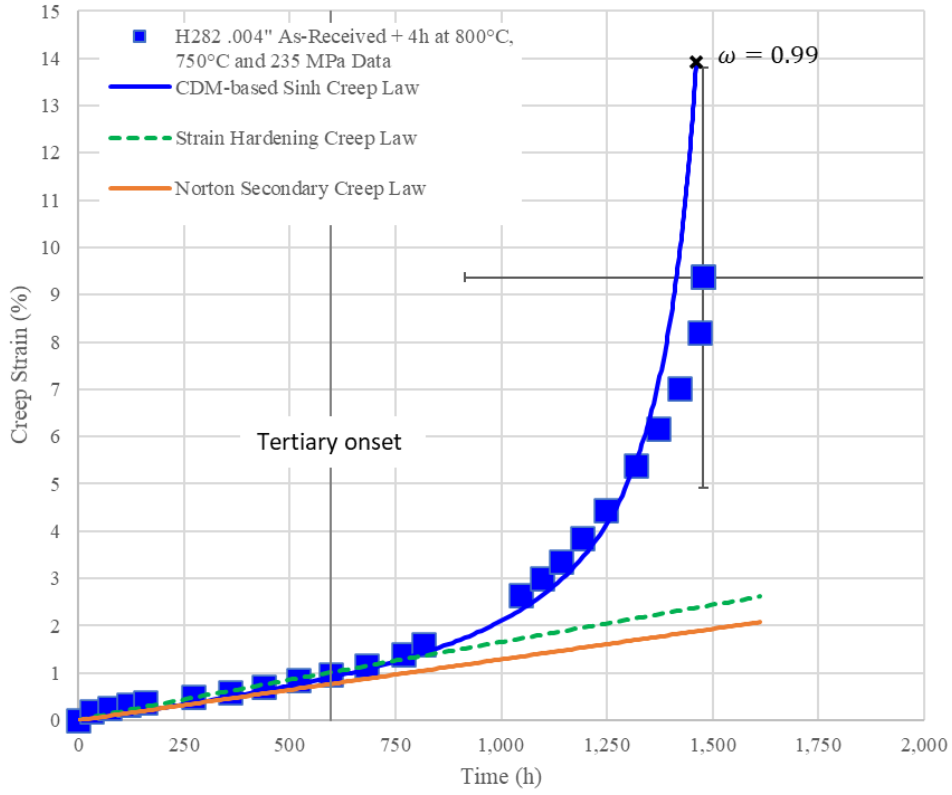

Figure 26: Creep data and modeling approach comparisons

The Sinh creep law has been calibrated using the Haynes 282 code case and the data generated under Task 2. A representative example of the model being exercised is provided in Figure 27. The following lettered-list mirrors Figure 27 subfigures:

a) Example graphic of an as-manufactured flat-crest Haynes 282 test article. The following simulation graphics are indicative of the single highlighted fin.

b) Simulation contour of the SE024 damage parameter (omega) under test conditions at the simulated failure time. Simulated failure is interpreted when the damage parameter equates to unity (shown as red in the contour). The life-limiting-location in this test article is nearest the brazed-joint and fin interface through the fin parent material. Interestingly, note that if manufactured appropriately, failed samples should exhibit parent material rupture. This concept will be revisited in the failure analysis sections.

c) The simulation contour of SE024 accumulated creep strain at failure shows approximately 10% maximum creep strain. This agrees with the Haynes 282 code case and the Task 2 results. Note that the fin loading is almost entirely in the principal tensile orientation.

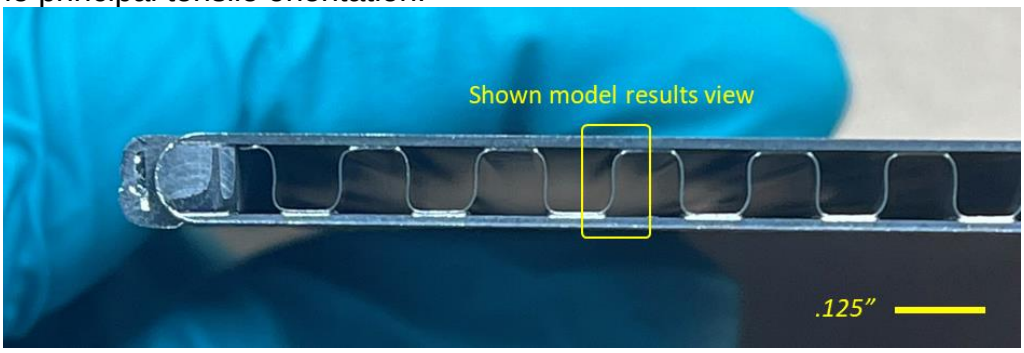

(a)

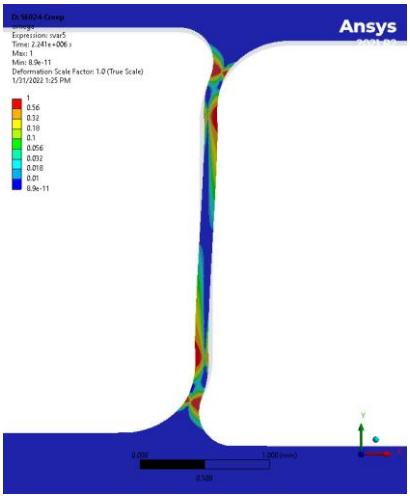

(b)

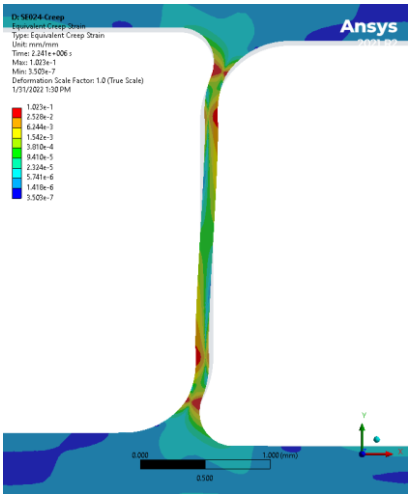

(c)

Figure 27: SE024 as-manufactured and simulation of creep test results (a) As-manufactured geometry (b) damage parameter omega at failure (c) creep strain at failure

A summary of completed and on-going pressurized creep tests is provided in Table 15. A total of 9 tests were completed successfully. All test articles were charged with CO2 and

held at 750°C. Maximum charge pressures approached 45 MPag and maximum creep rupture lifetimes are approaching 7,000 hours, and expected to approach 10,000 hours. The test matrix includes a variety of fin types and surface preparation techniques to explore the nuances each embodies. Overall, much was learned and a quality matrix was produced to yield confidence that life modeling and manufacturing practices are in agreement. Additionally, the as-manufactured hardware has been demonstrated at temperature and pressure representative of supercritical CO2 power cycles yielding a positive outlook for the technology.

Table 15: Pressurized creep test article specifications and results

i	Sample ID	Foil thk (in)	Fin type	Fin density	Status	Surface Prep.	Temp. (°C)	Pressure (MPag)	Start	Rupture (h)
1	SE007	0.004	round crest, comp.	55	Complete	Alcohol, Pickle	750	10.3	07/07/21	247
2	SE019	0.004	round crest, comp.	55	Complete	Alcohol, Pickle	750	11.7	07/19/21	38
3	SE024	0.004	flat crest	8	Complete	Alcohol, Pickle	750	4.8	10/25/21	312
4	SE029	0.004	flat crest	8	Complete	Alcohol, Pickle	750	8.3	11/15/21	1667
5	SE030	0.008	round crest	35	Complete	Alcohol, Pickle	750	44.8	11/15/21	1525
6	SE017	0.004	round crest, comp.	55	Complete	Alcohol, Pickle	750	22.8	07/07/21	5664
7	SE018	0.008	round crest	35	On-going	Electrolitic Ni-Plated	750	22.8	07/28/21	6894+
8	SE033	0.004	flat crest	8	On-going	Alcohol, Pickle	750	5.5	02/01/22	2472+
9	SE036	0.004	round crest, comp.	55	On-going	Alcohol, Pickle	750	22.8	02/01/22	2472+

Results from the described simulation and measurement exercising this model with the gathered test data are shown in Figure 28. The figure is presented as simulated failure versus measured failure in units of hours. A line-of-perfect fit is provided along with a plus and minus confidence interval at 1-sigma and 3-sigma as defined by the Haynes 282 code case. A total of 6 (67%) are likely to fail within the 1-sigma scatter band, 88% have (or are likely to) fail within the 3-sigma scatter band, and all samples have/are-likely to fail within the 4-sigma scatter band.

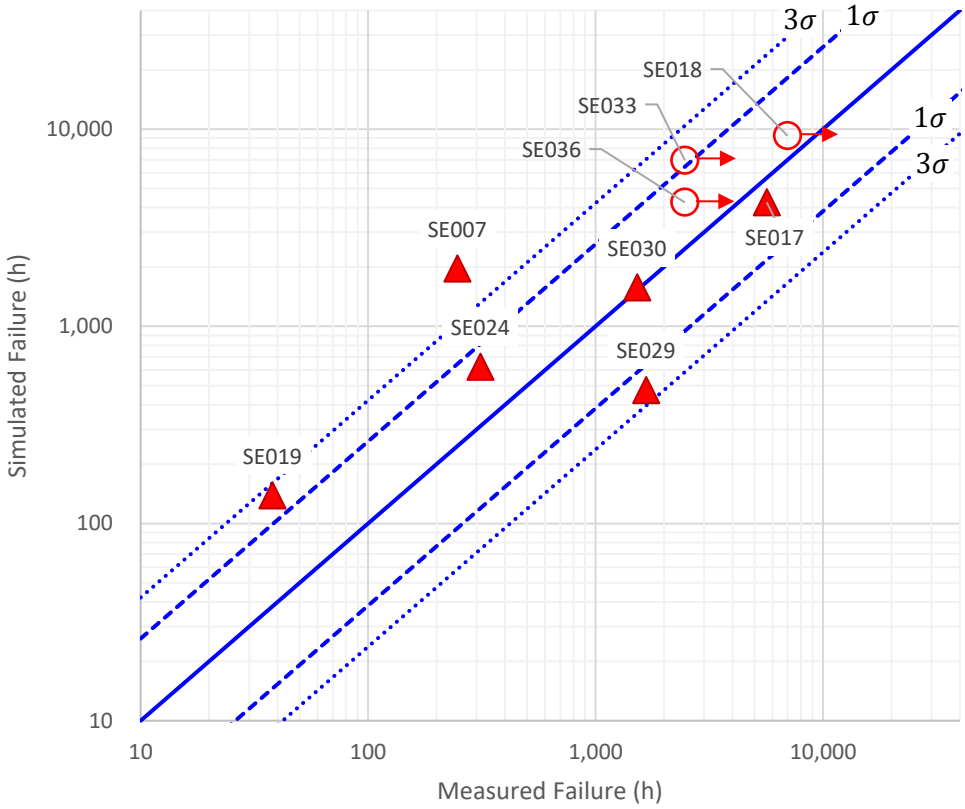

Figure 28: Simulated verses measured failure time in hours

Milestone 1.3.2 and 2.3.3

Table 16: Detailed Milestones 1.3.2 and 2.3.3

M #	Milestone Title	Description	Metric	Success Value	Assessment Tool	Metric Justification
1.3.2, 2.3.3	Creep characteristics - processed plate-fin	Construct typical and (-)3σ σ-t_r and LMP. Use uniaxial test data and existing thick sheet and plate database as benchmark.	Creep-rupture LMP uncertainty	<5%	Uncertainty analysis considering variables in geometry, operating conditions, and test setup	Quantified uncertainty of critical design parameter. Typical variance of large thick-sheet and plate datasets is 1-3%
			Creep-rupture LMP standard deviation	<250 LMP	95% confidence interval based on measurement deviation from power-law trend line	Typical standard deviations of relevant large datasets exist between time-temperature values of 50 and 200
			Form thickness debit uncertainty from thick sheet and plate datasets	< 15%	95% confidence interval on departure from thick sheet and plate behavior	Debit from creep-rupture performance of thick sheet and plate is expected. Ability to quantify departure is a necessary design parameter

Life quantification methods switched from the elastic LMP method to the inelastic Sinh creep model. Milestone metrics are therefore reported with respect to *Figure 28* instead of *Figure 10*.

- Time to failure is a measured parameter and therefore negligible.
- Standard deviation from the line of perfect fit is 41%. The 95% confidence interval yields 82%.
- The form thickness debit from Milestone 2.2.3 is inherent in the material model used and therefore not applicable here.

v. Subtask 3.5: Pressurized creep failure analysis

Graphics of SE024 post-failure are provided in Figure 29 and Figure 30. The following numbered and lettered lists correspond to Figure 29 and Figure 30 and subfigures or annotations:

1. Figure 29
    a. High-level test article graphic showing the top-side parting plate having ballooned open upon failure.
    b. A perspective graphic inside of the ballooned unit cell showing rupture between the fin and both top/bottom plates. The fin waves are indicative of fin stretch and relaxation pre and post failure respectively.
    c. Callout to a fin that is still bonded to the bottom plate and parent material rupture along the height of the fin.
2. Figure 30
    a. SE024 micrograph of an intact fin post failure
    b. SE024 micrograph on a rupture fin post failure
    c. The denoted red region is indicative of the braze-fillet region
    d. The brazed fillet discoloration is indicative of chromium depletion, parent material does not show a similar effected thickness. The flat-crest brazed joint is fillet is measured at 0.010".
    e. A brazed joint eutectic.
    f. A small void is observed between the fin and plate, fortunately, structural implications are likely minimal in this form and location.
    g. Indicative of the simulated life-limiting-location (Figure 27), this is supported by Figure 30b. This observation is an important bridge between the test results and the simulation results.
3. Figure 31 - A line scan shows that that generally, the braze material is enriched in nickel and depleted in all other elements when compared to the fin and plate. Fin Aluminum and Titanium compositions are approximately 1.2 and 1.99 respectively. Both are on the lower end of UNS NO7208 bounds, likely due to brazed joint diffusion. Braze joint compositions are 0.60 and 0.54 respectively.

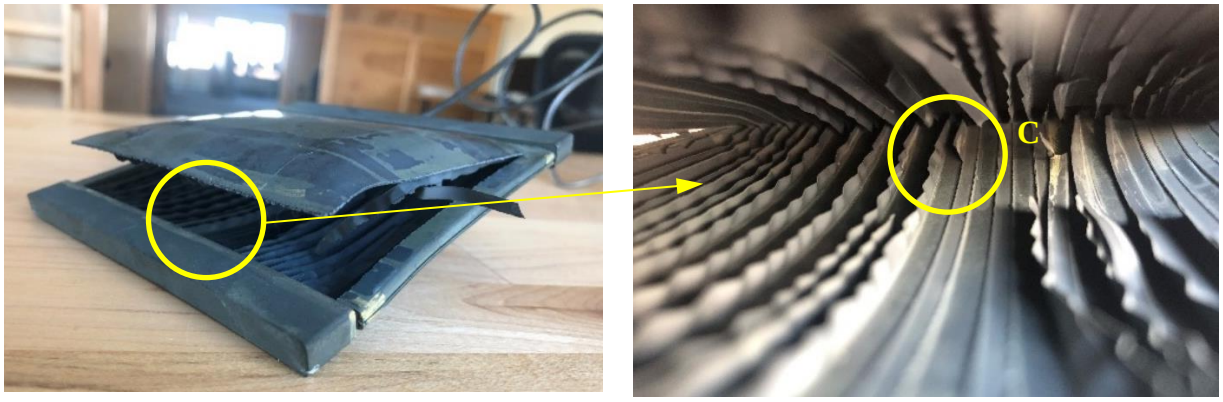

(a) (b)

Figure 29: SE024 macro-failure graphics

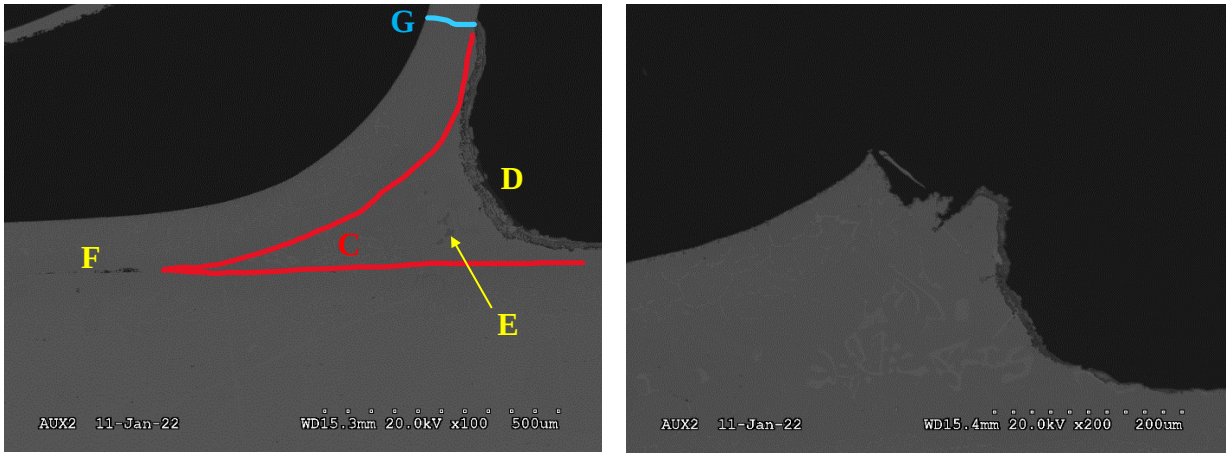

(a) (b)

Figure 30: SE024 micro failure graphics

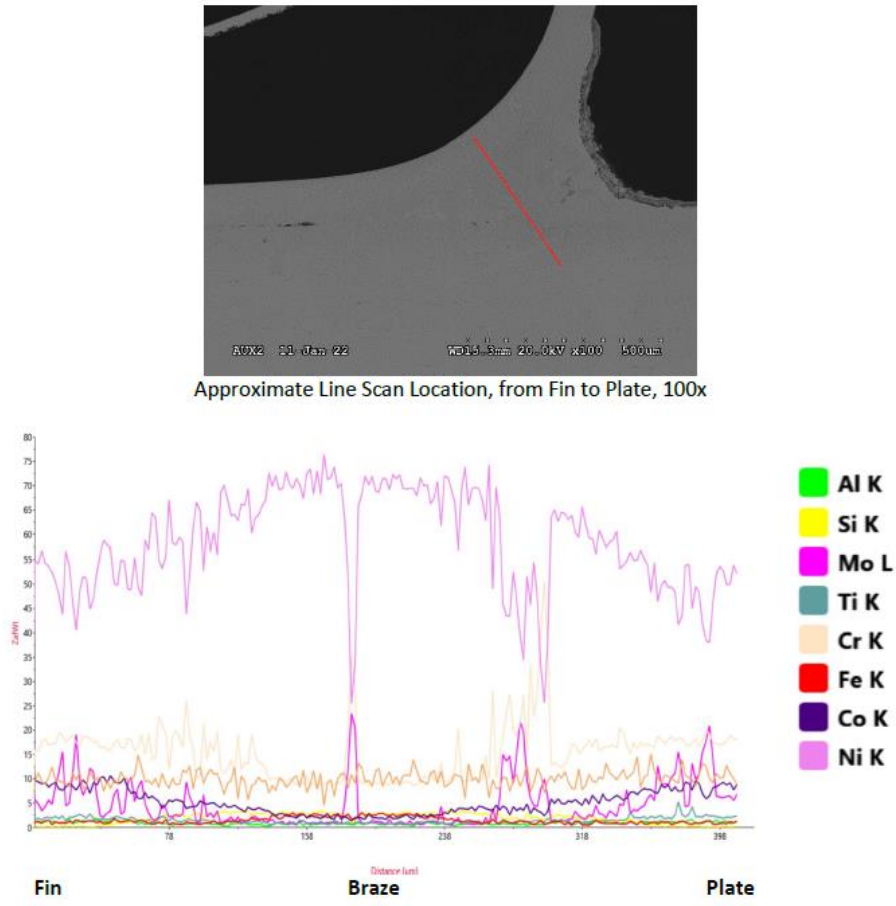

Figure 31: SE024 EDS line scan

vi. Subtask 3.6: Pressurized creep-fatigue testing

The creep-fatigue testing campaign is analogous to the pressurized creep testing campaign except, pressure is cycled. A representative data from a single fatigue cycle (i) is shown in Figure 32. The is at isothermal temperature, pressure is ramped (10 seconds) from zero to test spec pressure, pressure is held for 10 minutes, the pressure is vented (1 second), and the process repeated. A few nonlinearities are observed. During the first seconds of the charge ramp, pressures spikes to 500 psi before settling into a steady state ramp rate. And a small pressure drift is observed from cycle start to end. Both phenomena are attributed to system volumes, system hardware, and transient thermal implications of a compressible fluid.

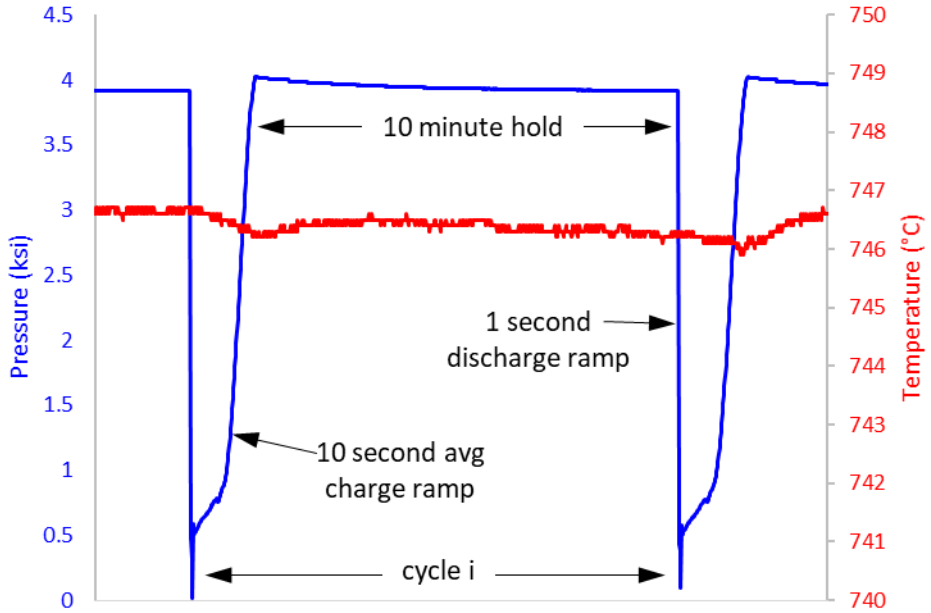

Figure 32: Representative creep-fatigue cycle characteristics

Measure pressure and temperature are extracted from the test results and used to simulate the stress-strain response of the test article hardware. The simulation results are then interpreted using the total strain range approach. The total strain range accounts for elastic, plastic, creep, and thermal strains endured each cycle, according to the following:

$$\Delta\varepsilon_{total} = \varepsilon_{elastic} + \varepsilon_{plastic} + \varepsilon_{creep} + \varepsilon_{thermal} \quad (5)$$

In all cases, strains are extracted from a transient finite-element model specific to the as-manufactured geometry and measured test conditions.

A summary of the creep-fatigue testing campaign is provided in Table 17.

Table 17: Pressurized creep-fatigue test article specifications and results

i	Sample ID	Foil thk (in)	Fin type	Fin density	Status	Surface Prep.	Temp. (°C)	Pressure (MPag)	Start	Cycles (-)
1	SE025	0.004	round crest, comp.	55	Fail	Alcohol, Pickle	750	12.4	11/02/21	-
2	SE026	0.008	round crest	35	Complete	Electrolitic Ni-Plated	750	18.6	11/10/21	3477
3	SE027	0.008	round crest	35	Fail	Electrolitic Ni-Plated	750	24.8	11/10/21	-
4	SE031	0.004	flat crest	8	Complete	Alcohol, Pickle	750	4.8	01/29/22	168
5	SE032	0.008	round crest	35	Complete	Alcohol, Pickle	750	24.8	11/10/21	1627
6	SE034	0.004	flat crest	8	Complete	Alcohol, Pickle	750	4.8	01/29/22	2589
7	SE035	0.004	round crest, comp	55	On-Going	Alcohol, Pickle	750	5.5	02/16/22	8725
8	SE025	0.004	round crest, comp	55	Queued	Alcohol, Pickle	750	12.4	TBD	TBD

- The five completed and on-going samples are compared with open-source Haynes 282 fatigue data in *Figure 33* at relevant temperatures. It is important to note that the shown literature data is pure fatigue and the data collected in this program is creep-fatigue with a 10-minute hold. The reported strain range for the Subtask 3.1 test article is a result of FEA modeling under the stated test conditions. At a strain range of 0.4%, the creep-fatigue data shows about one order of magnitude debit in cycles to failure. Haynes 230 creep-fatigue has been shown to reduce cycles to failure between 50% and 90% with a 10-minute hold [27].
- One sample is queued for testing.
- Two samples

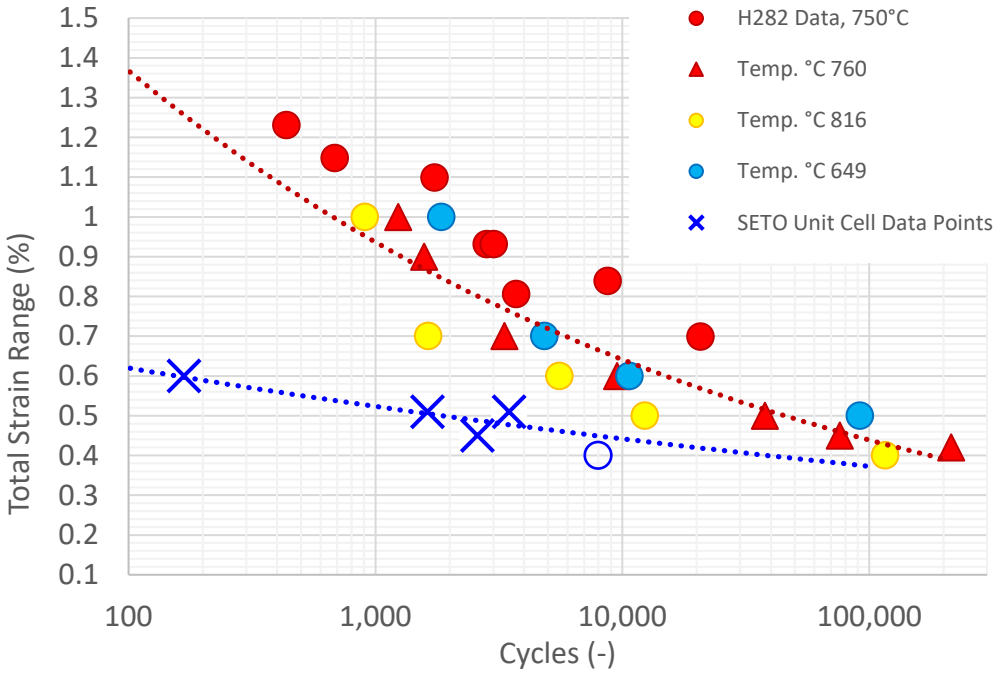

Figure 33: Creep-Fatigue intermediate results and data compilation [5]

Milestones 1.3.4 and 2.3.5

Table 18: Detailed milestones 1.3.4 and 2.3.5

M #	Milestone Title	Description	Metric	Success Value	Assessment Tool	Metric Justification
1.3.4, 2.3.5	Creep-fatigue characteristics – processed plate fin	Construct typical and (-)3σ Δεt-N curve and t-N curve. Use existing thick sheet and plate database as benchmark.	Strain-range uncertainty	<15%	Uncertainty analysis considering variables in geometry, operating conditions, and test setup	Quantified uncertainty of critical design parameter.
			Cycles-to-failure uncertainty	<50%	Uncertainty analysis considering variables in geometry, operating conditions, and test setup. 95% confidence interval based on variance in test data about elastic and plastic Manson-Coffin laws	Cycles to failure for a provided strain range is required in life estimate. Plus or minus 50% is a generally accepted margin for fatigue cycles-to-failure.
			Form thickness debit uncertainty from thick sheet and plate datasets	< 15%	95% confidence interval on departure from thick sheet and plate behavior	Debit from creep-fatigue performance of thick sheet and plate is expected. Ability to quantify departure is a necessary design parameter

- FEA resultant strain range uncertainty considering geometric tolerances and temperature and pressure measurements is less than 10%.
- Confidence in cycles to failure remains at +/-50% as a best case scenario for dataset scatter.
- The form thickness debit is inherent in the material model developed, nothing to report here.

vii. Subtask 3.7: Pressurized creep failure analysis

All fatigue samples have demonstrated some form of optically visible failure mode. Similar conclusions made about parent material failure in the creep-failure sections are applicable here. Fatigue sample SE026 (Figure 34) was arguably the most explosive failure Brayton has ever recorded. Parting plates are observed as blow-off on both sides and parent material failure is observed throughout and at all interfaces. Similar imaging and EDS analysis was conducted.

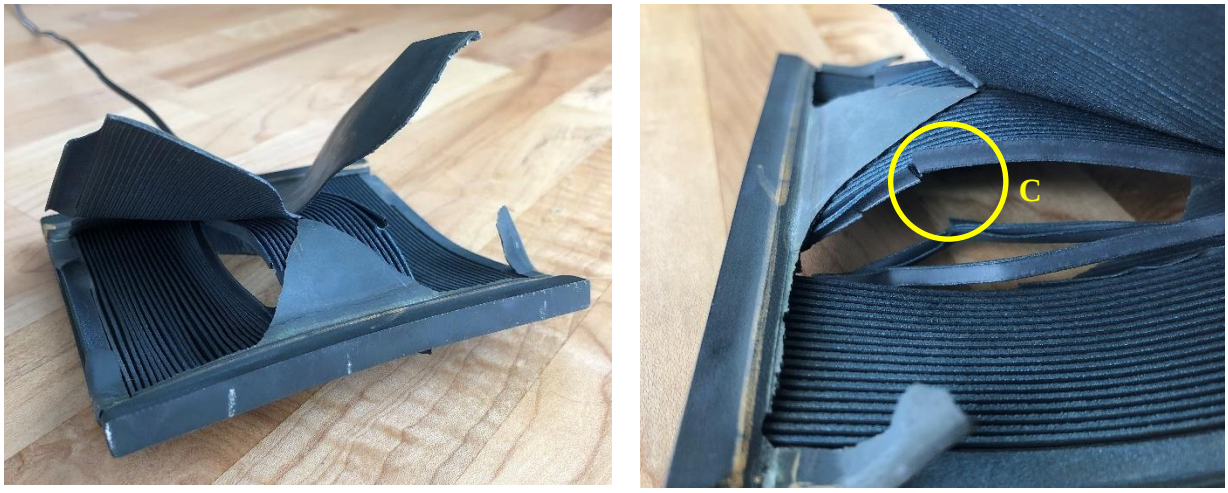

(a) (b)

Figure 34: SE026 creep-fatigue macro failure graphics

viii. Subtask 3.8: Heat exchanger application benchmarks

This subtask aims to provide motivation behind the rather fundamental and foundational work presented in all preceding tasks and ground the results in heat exchanger practice as pertains to supercritical CO2 in Concentrated Solar Power but also ancillary applications. For a benchmark, the Brayton Energy GEN3 Gas-Phase proposal for a counterflow supercritical CO2 to silica sand particle Thermal Energy Storage (TES) heat exchanger constructed with Haynes 230 will be used. The specifics of this heat exchanger will be developed throughout this section and compared to a similar heat exchanger assuming Haynes 282 construction. The superior material characteristics of Haynes 282 are exploited to recommend an alternative geometry using Haynes 282 assuming equal thermal-hydraulic and lifetime requirements to the Haynes 230 construction. Cost metrics for the Haynes 282 construction is very much a work-in-progress given the early stages of manufacturing development, but attempt is made at a $/UA comparison.

It should be noted that this section assumes a successfully developed manufacturing process for Haynes 282 and achievable material properties equivalent to existing thick from database. As testing results mature, this assumption stands for revisiting.
The flow conditions used in this section represent thermal energy storage in the form of accepting sCO2 at 730°C and 25 MPa from a solar receiver and heating silica sand particles initially at 565°C to 715°C.

Heat Exchanger Definition

The general heat exchanger architecture concept considered here consists of a multiplicity of unit cells in parallel joined together via tube and manifold (see Figure 35). With this approach, the behavior of each unit cell is largely independent at elevated temperature and construction allows for modular quality-control and assembly. The unit cell flow configuration features sCO2 and particles in counterflow, Figure 35 Section A-A gives 2-D callout to this flow configuration. This 2-D graphic will be referenced throughout this section as the characteristic unit cell geometry. Dimensions are provided for scale reference only.

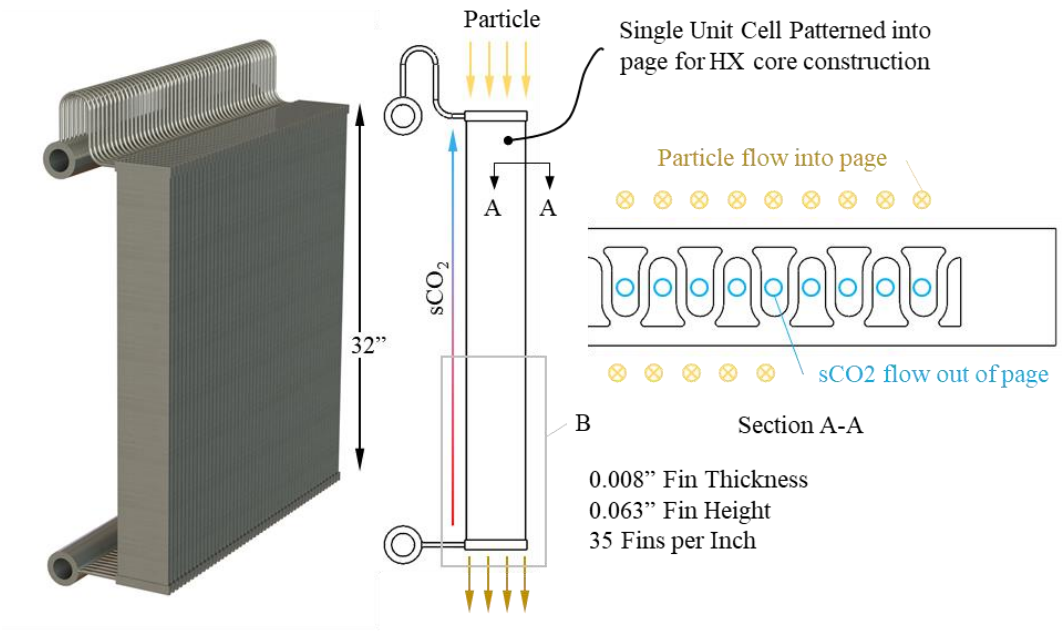

Figure 35: Heat Exchanger Modeling Concept

The following sections aim to highlight key modeling elements prior to arriving at a specified heat exchanger geometry, performance, and cost. These topics are broken down in to Thermo-Mechanical, Thermo-Hydraulic, and Cost Modeling constituents.

Thermo-Mechanical Modeling

The thermo-mechanical modeling process begins with coupled thermal and structural analysis to understand geometry combinations capable of service in the application environment. This is an iterative process that ultimately ends with transient analysis to quantify creep and fatigue life expectations. For purposes of this report, the two following highlights are provided for context.

1. Transient Thermal Analysis

A transient thermal analysis of a single unit cell is shown in Figure 36, temperature contours are representative of the sCO2 inlet as indicated by Figure 35B. The transient analysis features a 10°C/s ramp rate from 730°C to 580°C and contours are shown at 20 second increments between 0 and 100 seconds. Figure 36A (at the 100 second timestamp) highlights the notable thermal transient behavior of this architecture, where fluid temperature is 580°C (blue) and header block and edge bar metal temperatures are of slightly greater temperature. Thermal response of the fin structure is almost immediate and thermal response of the thicker features lag. In transients like this, typical life limiting locations exist in the region denoted by Figure 36A.

2. Transient Structural Analysis

Using the developed thermal transient results, a macro-scale elastic transient structural and sub-model of life-limiting regions are developed to quantify stress and strain for creep and fatigue life calculation. The sub-model of the life-limiting location (Figure 36A), is shown in Figure 37, where sub-model remote boundary conditions are

representative of the macro-scale unit cell response and applied to the locally specified geometry. Figure 37 component descriptions are as follows:

- Figure 37a: Imported sub-model thermal profile and charge pressure are applied to the shown geometry
- Figure 37b: Resultant stress profile in the terminal fins at time equal to 18 seconds.
    - b.1: Indicative of the creep life limiting location.
    - b.2: Indicative of the fatigue life limiting location.
- Figure 37c: Representative stress profile at the b.1 plane. Note peak stresses exist near the brazed joint and fin crest.
- Figure 37d: The method for elastic FEA creep life estimation consists of averaging the thru-wall bisection stress as indicated in the figure. The theory being that over time, peak stresses relax and normalize to the average.

The time history of peak stress in the Figure 37b terminal fins is shown in Figure 38. At time equals zero, the heat exchanger cell is in steady state operation. At time equals approximately 18 seconds, stress peaks due to the thermal gradients apparent in the header-block/edge-bar/finned structure. The stress (or strain) range used in fatigue calculation is indicated by label A and the creep strain used in creep life calculation is indicated by the area under the transient curve, label B. Both of these measurements are inputs to the linear summation of creep and fatigue damage as required by the ASME BPVC code (Equation 2)

$$\sum_{i}^{n} \frac{n}{N_d} + \sum_{j}^{m} \frac{\Delta t}{T_d} < 1 \qquad (2)$$

Where n and N_d are the number of cycles of type i and the allowable number of cycles of type i and Δt and T_d are the actual time at stress intensity k and the allowable time at stress intensity k.

Indications of time-to-steady-state and Haynes 282 yield strength are referenced on the figure for reference only.

Figure 38 annotation C is indicative of what to expect from time-dependency in this elastic model. The peak bisection stress and average bisection stress from Figure 37d are plotted on this figure. Over time, the peak stress will relax to the average value but transient behavior is to be maintained.

Given these analysis, roughly thermo-mechanically equivalent characteristic unit cell microstructures for Haynes 230 and Haynes 282 are presented in Figure 39. These characteristic geometries are representative of the Figure 35 heat exchanger architecture and the plate and fin construction. The Haynes 282 geometry is visual less dense than the Haynes 230 counterpart, meaning less material is needed to contain the sCO2 25MPa charge pressure. This is in large part due to the structural advantages of Haynes 282 at 730°C. For reference, ASME allowable stress for Haynes 282 at 730°C is 138 MPa whereas allowable stress for Haynes 230 is 59 MPa.

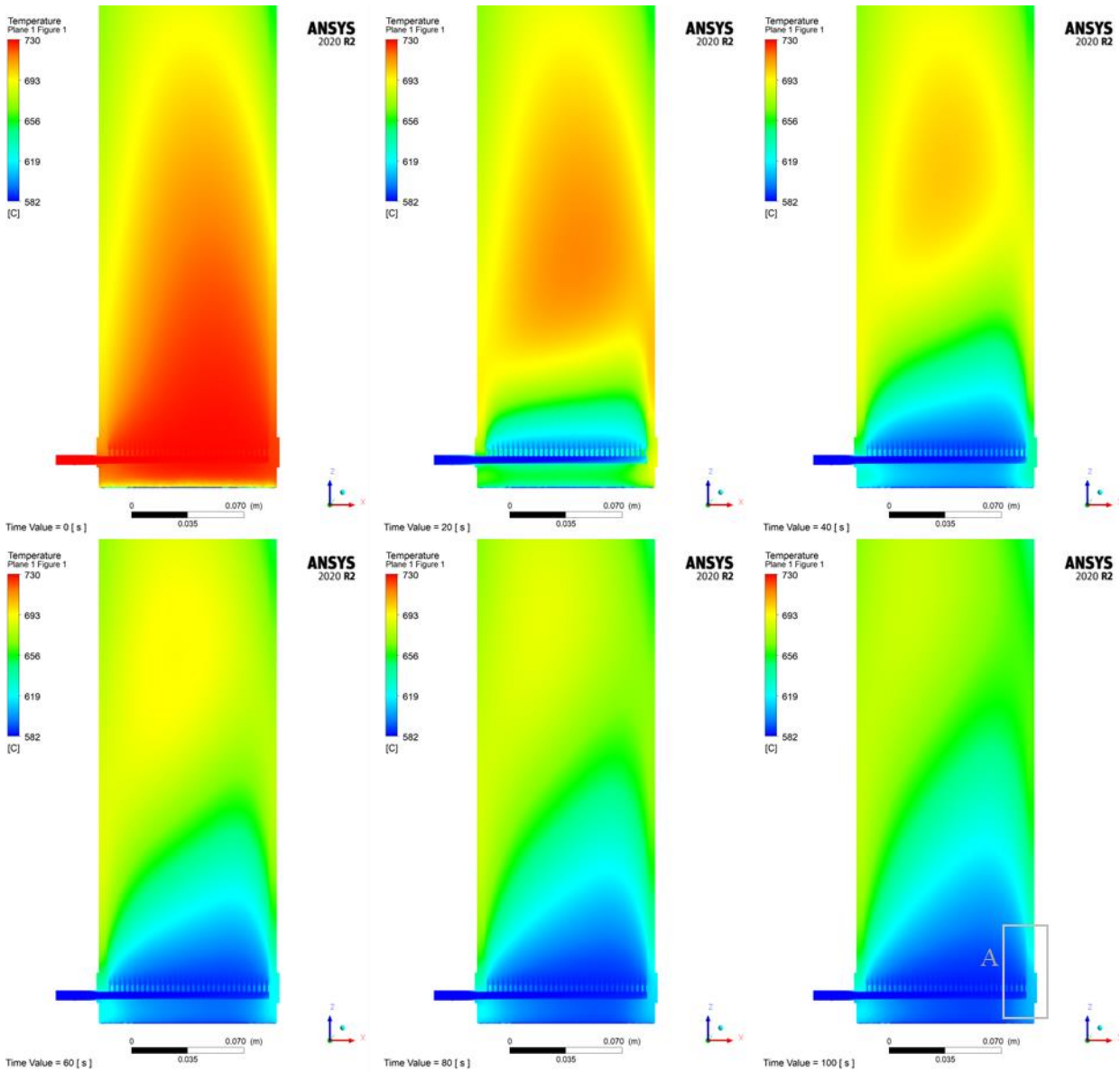

Figure 36: Transient Thermal Analysis Time History

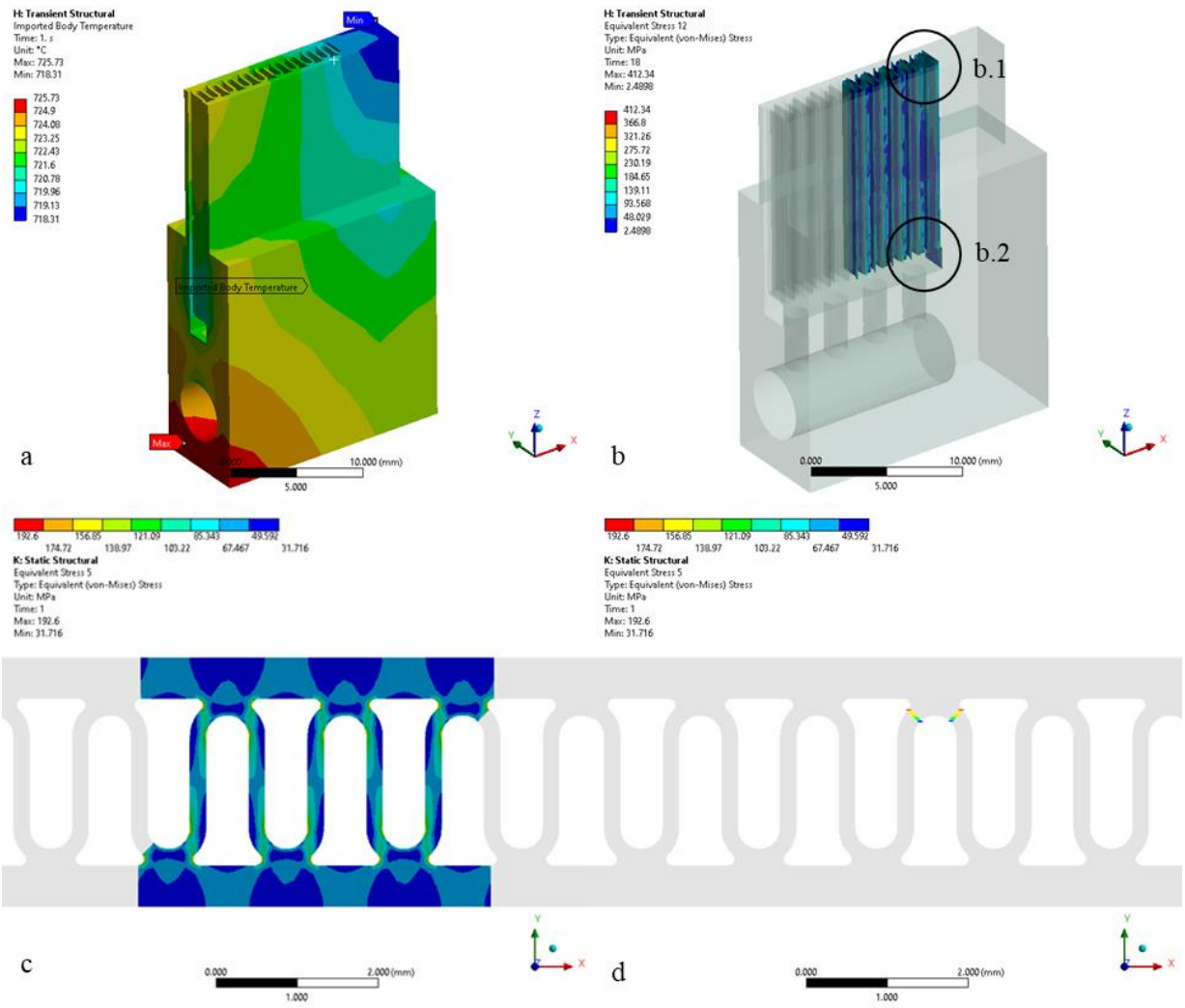

Figure 37: Transient Structural Analysis Snapshots

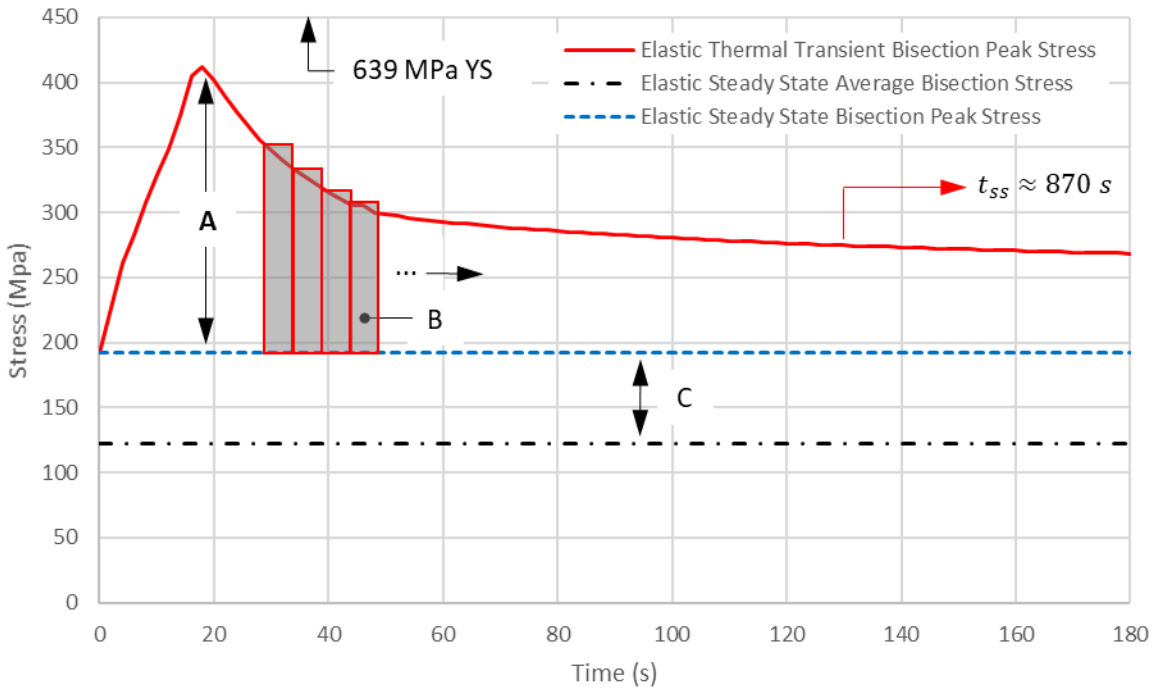

Figure 38: Transient Structural Stress Time History

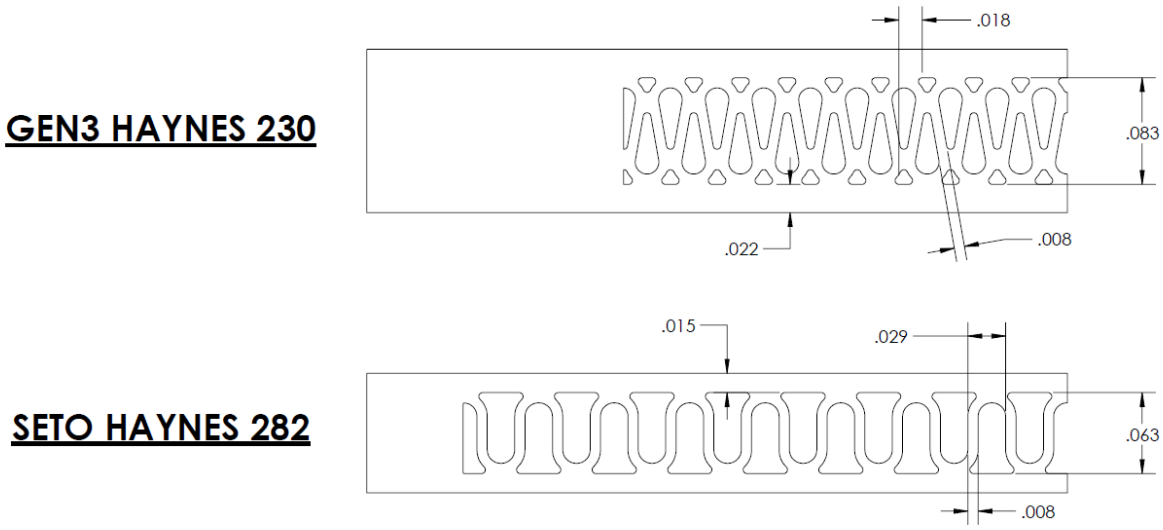

Figure 39: Haynes 230 and Haynes 282 thermo-mechanically equivalent geometrics

Thermo-Hydraulic Modeling

A numerical heat exchanger model employing discretized ε-NTU sub-heat exchangers for overall heat exchanger performance has been developed as described in *Heat Transfer Section 8.6.3* by Nellis and Klein with application to this TES problem. This heat exchanger modeling approach was selected in attempt to adequately reflect the implications of temperature dependent CO2 and particle material properties. The described model has been benchmarked using previous testing campaigns on recuperators at Brayton Energy, most notably the GEN3 Phase 2 TES heat exchanger. The structurally possible geometries developed in the previous section represent a realistic and critical input to the thermal-hydraulic model. For now, geometry combinations have been limited to the Haynes 282 0.008" given the realistic initial testing with the product form. Future iteration might prefer the 0.004" product form. Assuming the GEN3 Gas-Phase Charging TES heat exchanger performance requirements as a fixed output, the most critical output from this thermo-hydraulic modeling effort is relative heat exchanger size (mass and unit cell count) to achieve the same performance. A side-by-side comparison of the GEN3 Haynes 230 Baseline and the SETO (this work) Haynes 282 Baseline is presented in Table 19. The list of model constants is presented in Table 19. Because the CO2-to-particle heat exchanger is largely particle-side convection limited (Conv. Resist. Ratio = Particle-Side Convection Resistance divided by CO2-side convection resistance), the reduction in fin density enabled by the superior strength of Haynes 282 shows approximately 38% reduction in heat exchanger metal mass to achieve the same performance requirements (effectiveness and pressure drop). Translation of this mass reduction to cost reduction is appreciated in the next section.

Table 19: Thermo-Hydraulic Modeling Results

		Case	
Parameter	Unit	GEN3 Haynes 230 Baseline	SETO Haynes 282 Baseline
Material	-	H230	H282
Cell Width	m	0.2032	0.2032
Fin Height	in	0.083	0.063
Fin Thickness	in	0.008	0.008
Fin Density	fins/inch	55	35
Parting Plate Thk.	in	0.020	0.015
Cell Length	m	1.599	1.59
HX Mass	kg	1383.7	878.4
Normalized HX Mass	-	1.00	0.63
Cell Count	-	176	189
CO2 HTC	W/m2-K	906	841
Particle HTC	W/m2-K	370	370
Conv. Resist. Ratio	-	11.0	4.97

Constants	Unit	Value
Cell Width	in	8
Cell Length	in	64
Pressure Drop	%	0.05
Effectiveness	-	90
Flow Conditions	-	see HX def.
Microstructure	-	Fig. 26

Cost Modeling

The cost modeling process features a bottoms-up parametric approach where first costs are associated with raw material procurement and subsequent costs are incurred based on the intermediate processes involved prior to delivery of a heat exchanger core. This process summary is presented in Figure 40 where the process trees begin with a heat exchanger component in the raw form and the process lines denote required steps prior to first cell assembly (Figure 40 a, Figure 35 right) and then core assembly (Figure 40 b, Figure 35 left).

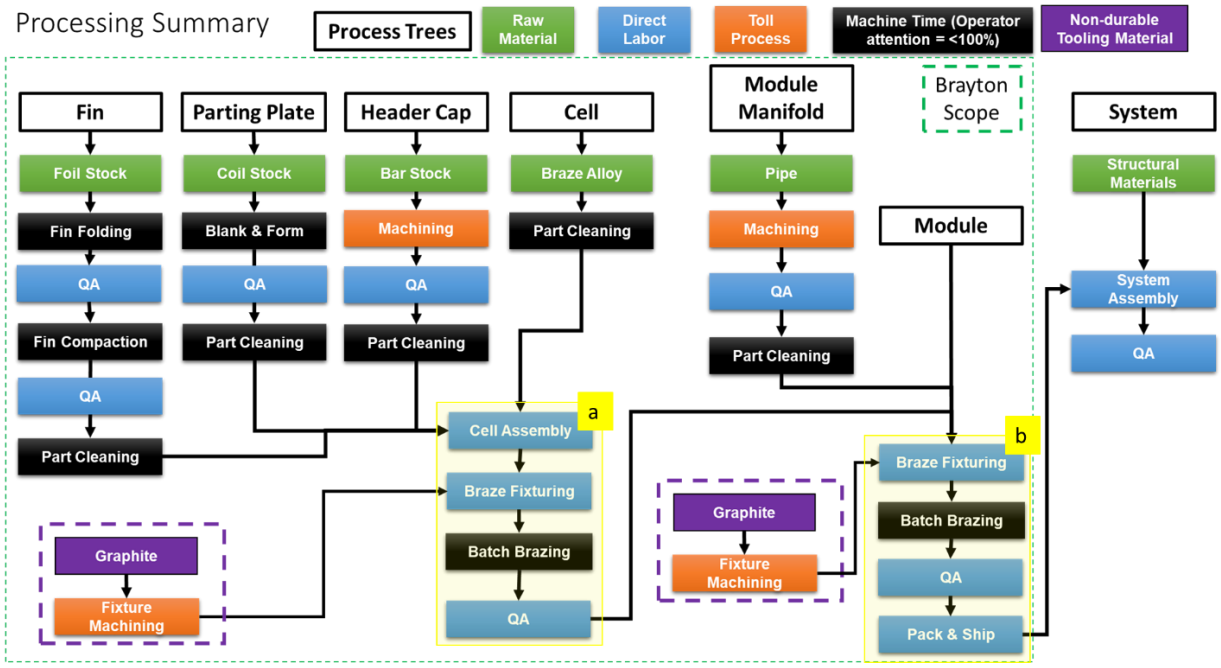

Figure 40: Unit Cell Manufacturing Processing Tree

Micro-sensitivities to the cost model include configuration details like flow width, length, height, fin density, material type, plate thickness, etc. Macro-sensitivities to the cost model include production, material, labor, and toll processing parameters. Items like yield/scrap rate, labor shifts, labor efficiency, throughput, market costs, order quantity, automation, and processing types are included at some level of detail. In general, the highest cost component for this architecture is the fin. Raw material costs are dictated by the supplier and require the most value added (rolling, heat treatment, and folding). It is for this reason, shifting from Haynes 230 to Haynes 282 is most advantageous in the described application.

Market costs of Haynes 282 and Haynes 230 are shown in Figure 41 where low quantity orders are indicated by LQ and similar cost is observed for both alloys in discussion. A cost item not yet appreciated in the cost model as described is the Electrolytic Nickel Plating as referenced in Subtask 3.2 discussion. A cost model for this plating process has been developed leveraging economies of scale and literature references (Figure

42). The nickel-plating model is currently being vetted through industry RFQ and discussion prior to implementation.

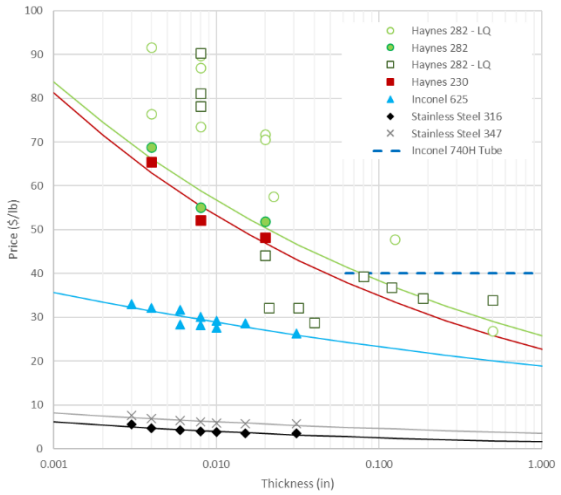

Figure 41: Alloy Market Costs

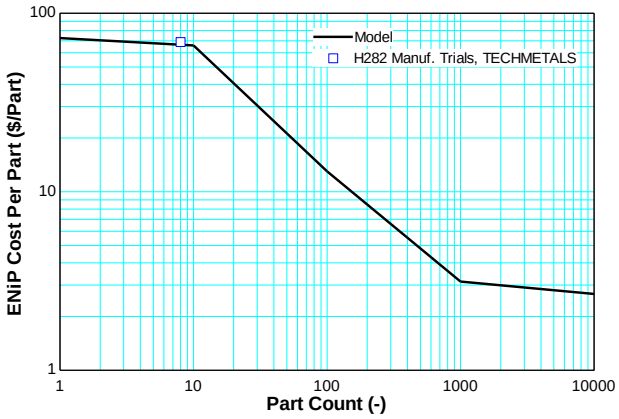

Figure 42: Electrolytic Nickel-Plating Economies of Scale

The cost break down for the Baseline Haynes 230 unit cell is shown in Figure 43. The high-pressure (HP) fin comprising approximately 38.6% of the total unit cell cost and plate comprising 19.3% (approximately 57.9% of total unit cell cost is associated with material costs of these two critical components). The Haynes 282 unit cell cost break down shows similar preference towards these two components with slightly more distribution towards header blocks. This behavior emphasizes cost reduction originating at the design level of these constituent components. To reiterate, the superior strength of Haynes 282 allows for sparse fin density and thinner plates, thus correlating to a direct cost savings.

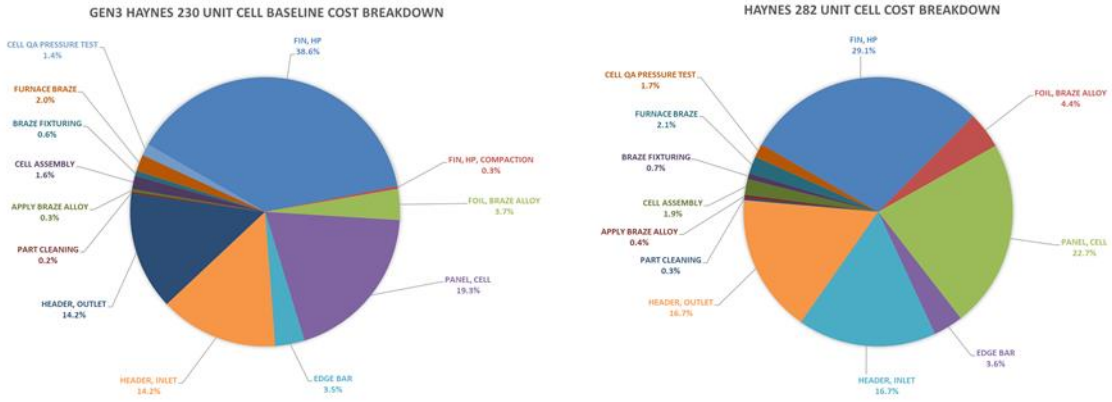

Figure 43: Unit cell cost breakdown by component and processing steps

Two scenarios for understanding the Haynes 282 cost savings over current state of the art are appreciated in Table 20. Two baseline cases are considered: 1 MWt and 100 MWt scale heat exchangers. The former is representative of a large-scale first-of-kind prototype and the latter representative of commercial-scale production with dedicated facilities and staff. The cost fraction associated with labor, materials, and toll processing is shown with correlation to heat exchanger scale. And the performance-weighted cost metric dollars per conductance ($/UA) is also shown as a model output. The associated costs savings at the prototype type scale and commercial-production scale represent 13.3% and 18.5% cost savings, respectively.

Table 20: Haynes 230 and Haynes 282 1 MW_t and 100 MW_t comparison

Material	Cost Fraction			Thermal Capacity, MW	$/UA	Cost Savings
	Labor	Material	Toll Proc.			
H230	0.06	0.36	0.58	1	9.4	-
H282	0.07	0.26	0.67	1	8.1	13.3%
H230	0.11	0.51	0.38	100	6.1	-
H282	0.14	0.40	0.47	100	4.9	18.5%

Milestone 2.3.6

Table 21: Detailed Milestone 2.3.6

M #	Milestone Title	Description	Metric	Success Value	Assessment Tool	Metric Justification
2.3.6	Heat exchanger design and modeling benchmark	Benchmark feasible PHX designs against currently employed technologies of similar and dissimilar form factors	Heat exchanger performance metrics Design Constraints: 100,000 hour creep-fatigue life $T_{f,out}$ > 700°C P_f = 25 Mpa	kg/UA, $/UA, allowable operating temperature and stress Comparison against heat exchangers using sufficiently characterized prior to this project	Analytical HX models, Brayton Energy Numerical HX models, CFD, FEA, ASME Pressure Vessel Code Section II, Section III, Section VIII, Section IX	Mass/cost weighted conductance is a normalizing comparison metric. For a required HX capability, how much material and how many dollars are required.

See *Table 20* above.

Milestone 2.3.7

Table 22: Detailed Milestone 2.3.7

M #	Milestone Title	Description	Metric	Success Value	Assessment Tool	Metric Justification
2.3.7	Stakeholder Briefing and Review	Brayton Energy and ORNL will engage industry stakeholders with vested interested in the manufacture and employment of candidate alloys characterized in this project. Special Metals, Haynes, Elgiloy, EPRI	Stakeholder Engagement	3-4 parties of interest. Special Metals and Haynes International are primary candidates as manufacturers, EPRI is a secondary candidate as an R&D institute, Elgiloy and Ulbrich are tertiary candidates as suppliers. Others may be identified later.	Dissemination of a technical review summary of fundamental and practical learnings will be provided up front. Follow up discussion will be welcomed in the form of education and future development.	The applied and focused nature of the data collected in this project merits engagement with alloy suppliers surrounding commercialization. Project learnings may aid in future developments and be advertised in brochure-like form.

There is open conversation with technical experts at ORNL, Eligiloy, Haynes International, Special Metals, and EPRI. A redacted final technical report will be disseminated to these stakeholders at project completion.

d. Missed Milestone 1.3.1

Table 23: Detailed Milestone 1.3.1

M #	Milestone Title	Description	Metric	Success Value	Assessment Tool	Metric Justification
1.3.1	Validate HX manufacturing process	Perform short-term tensile and pressurized life test of as-manufactured geometry and compare relative performance. Establish quantifiable benchmark between ASTM standard and pressurized test practice.	Creep-rupture percent difference (x3)	<25%	Comparison of Brayton Energy pressure-test apparatus with ASTM E139	Benchmark of pressurized creep and ASTM compliant tensile creep to create link between test practices. Repeated for 3 samples to identify trend/outliers
			Cycles-failure percent difference (x3)	<50%	Comparison of Brayton Energy pressure-test apparatus with ASTM E466, E606	Benchmark of pressurized creep-fatigue and ASTM compliant tensile fatigue to create link between test practices. Repeated for 3 samples to identify trend/outliers

- Tensile specimen manufacturing process steps revised after machining operation proved damaging to 4mil fin integrity.
- New coupons were manufactured but stack up of complete manufacturing steps resulting in runout of time. Brayton will find value in this effort and proceed with testing after project end

(a) (b)

Figure 44: Milestone 1.3.1 hardware graphics

6. Significant Accomplishments and Conclusions

End of Project Goals

Milestone Number	Milestone Title	Description	Metric	Success Value	Assessment Tool	Metric Justification
EOP-A	Creep-rupture benchmark	Material comparison of precipitation hardened stress rupture to solid-solution strengthened stress rupture. Precipitation hardened stress rupture is expected to yield favorable results, comparable to existing thick sheet and plate datasets.	100,000 hr rupture stress at constant temperature 95% confidence interval	>40%	Test data collected under this project and relevant previous. Non-dimensional time-temperature parameters will be used to scale data appropriately. Technical memo to be shared with DoE	Materials tested under this campaign will be compared to materials previously characterized. The material is to be determined. The temperature and stress are to be determined, a sweep or curve may prove most applicable.
EOP-B	Thermo-hydraulic benchmark	Performance comparison of comparable precipitation hardened to solid-solution strengthened heat exchanger topologies. Precipitation hardened stress rupture is expected to yield favorable life results suggesting less material or thinner gauges may be utilized. Both of which offer differing thermo-hydraulic benefits.	$/UA with 100,000 hr life and equal hydraulic penalty 95% confidence interval	>10%	Analytical HX models, Brayton Energy Numerical HX models, CFD, FEA, ASME Pressure Vessel Code Section II, Section III, Section VIII, Section IX. Technical memo to be shared with DoE	$/UA is a normalizing heat exchanger comparison metric, offering two of the more telling characteristics of the component - cost and conductance.

EOP-A: At 750°C and 235 MPa, nominal Haynes 230 plate ruptures in 18 hours whereas Haynes 282 4-mil foil ruptures in 500-2500 hours = 2-3 orders of magnitude

EOP-B: 18.5% cost savings when comparing Haynes 230 with Haynes 282 in a GEN3-type particle-to-sCO2 primary heat exchanger construction. Additionally, Haynes 282 would be capable of operating at a high TIT, offering cycle efficiency benefit and fortuning component and cycle engineers larger degree of freedom.

Final statements

- Haynes 282 foil is undeniably superior to previous state of the art solid-solution strengthened alloys. This has been quantified and supported by the fundamental development
- The practical development has demonstrated fabrication techniques that yield heat exchanger geometries with strength comparable to parent metal uniaxial strength.
- It was also shown that Haynes 282 heat exchanger constructions also provide long-term cost benefits over solid-solution strengthened counter-parts

Project Outputs

- Generated data to be made publicly available
- Stakeholders in nickel-foil manufacturing and application are to made aware of results

Budget and Schedule

All milestones, except one, complete over 23-month period of performance. Completed under budget and with adequate cost share.

III. Spending Summary by Budget Category							
	Approved Budget per SF-424A				Actual Expenses		
Budget Categories per SF-424a	BP 1	BP 2	BP 3	Total	Q1	Cumulative	%
a. Personnel	$162,300	$91,529	$0	$253,829	$23,357	$119,804	47%
b. Fringe Benefits	$0	$0	$0	$0	$0	$0	0%
c. Travel	$4,762	$4,762	$0	$9,524	$0	$0	0%
d. Equipment	$0	$0	$0	$0	$0	$0	0%
e. Supplies	$126,109	$0	$0	$126,109	$18,323	$118,900	94%
f. Contractual	$97,000	$83,000	$0	$180,000	$34,620	$189,690	105%
g. Construction	$0	$0	$0	$0	$0	$0	0%
h. Other	$0	$0	$0	$0	$696	$790	0%
i. Total Direct Charges	**$390,171**	**$179,291**	**$0**	**$569,462**	**$76,997**	**$429,184**	75%
j. Indirect Charges	$226,066	$117,824	$0	$343,890	$34,219	$171,765	50%
k. Total Charges	**$616,237**	**$297,115**	**$0**	**$913,352**	**$111,216**	**$600,949**	66%
DOE Share	$492,990	$237,692	$0	$550,682	$64,336	$470,731	85%
Cost Share	$123,247	$59,423	$0	$182,670	$46,880	$130,218	71%
Cost Share Percentage	24.9%	24.9%	24.9%	24.9%	42.2%	21.7%	

7. Path Forward

- The technology is technically sound, but the market needs affirmation in this non-traditional architecture for high-temperature, high-pressure applications.
- The path forward includes continued development in prototype and low-quantity production applications while the technology tries to find a home.
- The market is interested in the light-weight architecture and potential cost savings, investment in a code-qualification or larger scale demonstration is likely needed

Inventions, Patents, Publications, and Other Results

Publication in process pending at time of submitting this document.

8. References

[1] Maziasz, P. J., Shingledecker, J. P., Evans, N. D., Yamamoto, Y., More, K. L., Trejo, R., & Lara-Curzio, E. (2007). Creep strength and microstructure of AL20-25+ Nb alloy sheets and foils for advanced microturbine recuperators. *Journal of Engineering for Gas Turbines and Power*, *129*(3), 798–805. https://doi.org/10.1115/1.2718569

[2] Shingledecker, J. P. (2012). Metallurgical Effects on Long-Term Creep-Rupture in a New Nickel-Based Alloy. *Doctoral Dissertations*. Retrieved from http://trace.tennessee.edu/utk_graddiss/1348

[3] Purgert, R. et al. "Boiler Materials for Ultra Supercritical Coal Power Plants" Final Technical Report , Dec. 2015. DOE Award Number: DE-FG26-01NT41175, ODSA-OCDO Grant Number: D-05-02(A)

[4] Richard, C. et al. "Low Cycle Fatigue Evaluation for Regeneratively Coold Panels" NASA Contractor Report. Oct. 1971. Grant No. NAS 1-5002-4.

[5] He, J., Sandström, R., & Notargiacomo, S. (2017). Low-Cycle Fatigue Properties of a Nickel-Based Superalloy Haynes 282 for Heavy Components. *Journal of Materials Engineering and Performance*, *26*(5), 2257–2263. https://doi.org/10.1007/s11665-017-2586-x

[6] Boehlert, C. J., & Longanbach, S. C. (2011). A comparison of the microstructure and creep behavior of cold rolled HAYNES® 230 alloy™ and HAYNES® 282 alloy™. *Materials Science and Engineering A*, *528*(15), 4888–4898. https://doi.org/10.1016/j.msea.2011.03.019

[7] Rothman, M. F. (1990). Pressure vessel code construction capabilities for a nickel-chromium-tungsten-molybdenum alloy. In *American Society of Mechanical Engineers, Pressure Vessels and Piping Division (Publication) PVP* (Vol. 201, pp. 179–187). Publ by ASME.

[8] Purohit, A., Burke, W. "Elevated Temperature Creep Behavior of Inconel Alloy 625" 1984

[9] Mcmurtrey, M. D. (2019). Creep-fatigue Behavior and Damage Accumulation of a Candidate Structural Material for Concentrating Solar Power Solar Thermal Receiver (pp. 1–61).

[10] Ghoneim, A., & Ojo, O. A. (2011). Microstructure and mechanical response of transient liquid phase joint in Haynes 282 superalloy. *Materials Characterization*, *62*(1), 1–7. https://doi.org/10.1016/j.matchar.2010.09.011

[11] Sinclair, J. and Gyorgak, C. "Effect of Two Braze Coatings, Processing Variables, and Heat Treatments on 1200°F Stress Rupture Strength of L-605, A-286, and Inconel 700 Sheet" Oct. 1983.

[12] Khorunov, V. F., & Maksymova, S. V. (2013). Brazing of superalloys and the intermetallic alloy (γ-TiAl). In *Advances in Brazing: Science, Technology and Applications* (pp. 85–120). Elsevier Ltd. https://doi.org/10.1533/9780857096500.2.85

[13] Christensen, J., & Rorbo, K. (1974). NICKEL BRAZING BELOW 1025 C OF UNTREATED INCONEL 718. *Welding Journal (Miami, Fla)*, *53*(10).

[14] Eno, D. R., Young, G. A., and Sham, T.-L. "A Unified View of Engineering Creep Parameters." *Proceedings of the ASME 2008 Pressure Vessels and Piping Conference*. *Volume 6: Materials and Fabrication, Parts A and B*. Chicago, Illinois, USA. July 27–31, 2008. pp. 777-792. ASME. https://doi.org/10.1115/PVP2008-61129

[15] PCC Energy Group. (2014). *Inconel Alloy 740H: A Superalloy Specifically Designed for Advanced Ultra Supercritical Power Generation*. Retrieved from http://www.specialmetals.com/files/PCC EG 740H White Paper.pdf

[16] Haynes 230 Manufacturer Datasheet, Haynes International, 2019

[17] Haynes 282 Manufacturer Datasheet, Haynes International, 2019

[18] Inconel 625 Manufacturer Datasheet, Special Metals, 2019

[19] Liu, M., Zheng, W., Xiang, J. *et al.* Grain Growth Behavior of Inconel 625 Superalloy. *J. Iron Steel Res. Int.* **23,** 1111–1118 (2016). https://doi.org/10.1016/S1006-706X(16)30164-9

[20] Shingledecker, J.P., Pharr, G.M. Testing and Analysis of Full-Scale Creep-Rupture Experiments on Inconel Alloy 740 Cold-Formed Tubing. *J. of Materi Eng and Perform* **22,** 454–462 (2013). https://doi.org/10.1007/s11665-012-0274-4

[21] Kay, D. (2011, March). Brazing Base Metals Containing Small Amounts of Titanium, Aluminum. Retrieved from: https://vacaero.com/information-resources/vacuum-brazing-with-dan-kay/895-brazing-base-metals-containing-small-amounts-of-titanium-aluminum.html

[22] N. Bretz and C. Tennenhouse, AWS Welding Journal, Research Supplement, pp. 189s-193s, May, 1970

[23] Kay, D. (2014, February). Using Titanium "Getters"in Vacuum Brazing. Retrieved from: https://vacaero.com/information-resources/vacuum-brazing-with-dan-kay/1368-using-titanium-getters-in-vacuum-brazing.html

[24] Metglas High Performance Brazing Filler Metal Datasheet (2012) Retrieved from: https://metglas.com/wp-content/uploads/2016/12/Metglas-MBF-Product-Listing.pdf

[25] Stewart, C. M., 2013, "A Hybrid Constitutive Model for Creep, Fatigue, and Creep-Fatigue Damage," Ph.D. dissertation, University of Central Florida,Orlando, FL

[26] Haque, M. S., and Stewart, C. M. (February 23, 2016). "Finite-Element Analysis of Waspaloy Using Sinh Creep-Damage Constitutive Model Under Triaxial Stress State." ASME. J. Pressure Vessel Technol. June 2016; 138(3): 031408.

[27] Lu, Yen-Lan & Chen, L & Wang, G & Benson, M & Liaw, Peter & Thompson, S & Blust, J & Browning, P & Bhattacharya, A & Aurrecoechea, J.M. & Klarstrom, Dwaine. (2004). Hold-Time Effects on Low-Cycle-Fatigue Behavior of Hastelloy X Superalloy at High Temperatures. Proceedings of the International Symposium on Superalloys. 10.7449/2004/Superalloys_2004_241_250.